NSG-233

UNPUBLISHED PRELIMINARY DATA

SUI 64-40

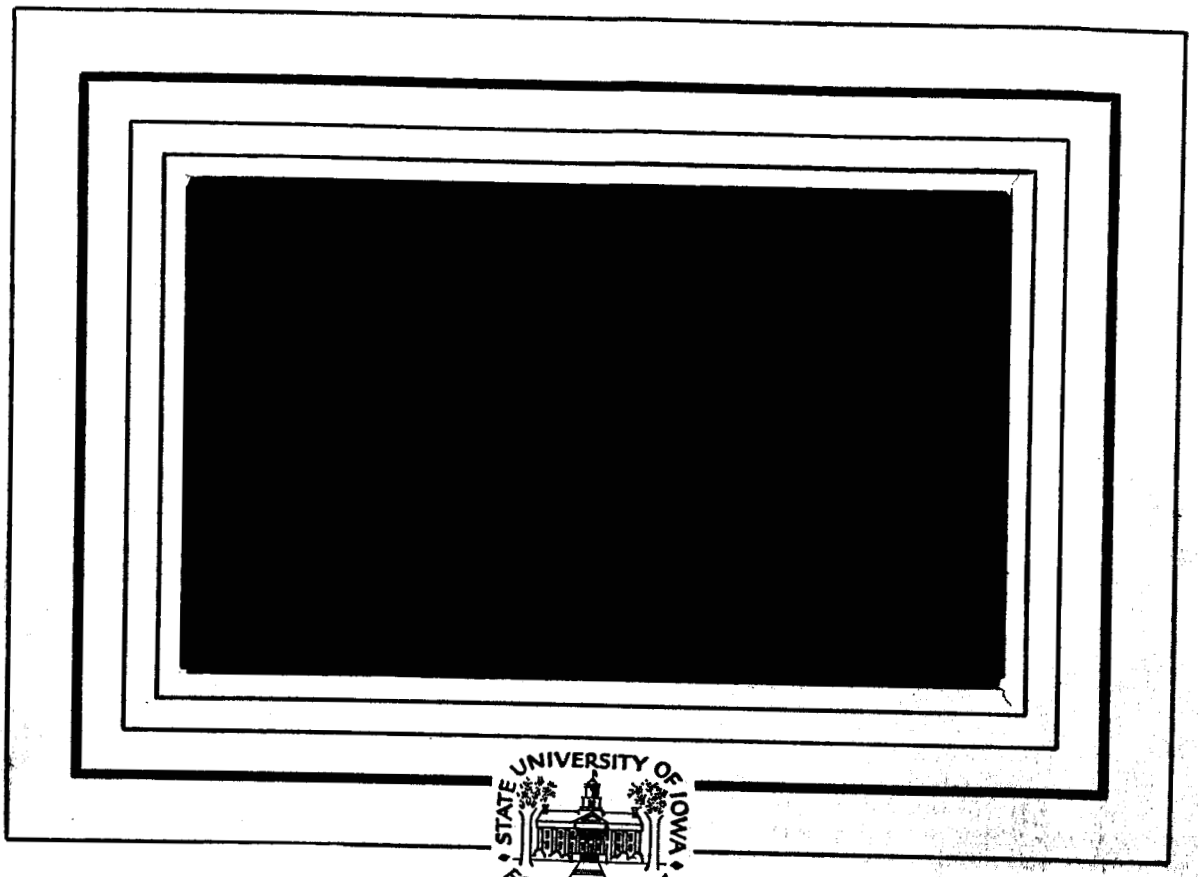

STATE UNIVERSITY OF IOWA
FOUNDED 1847

GPO PRICE $ _____

OTS PRICE(S) $ _____

	N65 17609 (ACCESSION NUMBER)		(THRU)
Hard copy (HC) 3.00	86 (PAGES)	1	(CODE)
Microfiche (MF) .75	CR 60905 (NSA CR OR TMX OR AD NUMBER)	29	(CATEGORY)

Department of Physics and Astronomy

STATE UNIVERSITY OF IOWA

Iowa City, Iowa

The Morphology of the Outer Zone Electron Distribution at Low Altitudes from January through July and September, 1963 from Injun III*

by

T. Armstrong**

*This work was supported in part by the U. S. Office of Naval Research under contract Nonr-1509(06).

**Graduate trainee of the National Aeronautics and Space Administration.

ABSTRACT

An intensive study has been made of data from three 213 G.M. tubes and one 302 G.M. tube which were carried on the State University of Iowa-Office of Naval Research satellite Injun III. Median latitude profiles of the electron population of the low altitude region of the outer zone for energies $E_e \gtrsim 40$ keV, $E_e \gtrsim 230$ keV, and $E_e \gtrsim 1.6$ MeV have been derived. Notable of the features of the median profiles are:

1. The large diurnal variation for $L \gtrsim 7.5$ for trapped and precipitated 40 keV electrons.
2. The lack of a sharply pronounced 'slot' for 40 keV electrons and the consequent softening of the integral electron spectrum around $L = 3.0$.
3. An apparent small diurnal variation of 230 keV trapped electrons for $6 \leq L \lesssim 8$.
4. A temporal change of ~ 1 order of magnitude in the intensity profile of 1.6 MeV electrons preceded and followed by periods of relatively stable intensity for $2 \leq L \lesssim 4.5$. This change occurred during a $K_p = 7$ magnetic storm which began on June 6, 1963.

The dependence of intensity on $|B|$ was investigated with the following results:

[redacted]
Code SC

DOCUMENT RELEASE FORM

3-16-65

DOCUMENT TRAVELER NO.:

TITLE: The Morphology of the Outer Zone Electron Distribution at Low Altitudes from January Through July and September, 1963 from Injun III.

ORIGINATING ORGANIZATION: State University of Iowa

SC No. 16 SE-2

ORIGINAL DOCUMENT NO.:

CONTRACT OR GRANT NO.: SC-NsO-233-62/16-001-002

SECURITY CLASSIFICATION OF DOCUMENT: Unclassified

DATE OF DOCUMENT:

TO BE COMPLETED BY TECHNICAL MONITOR:

Completion of this form will provide the Scientific and Technical Information Division with guidance concerning availability of the document identified above. Please return this original form to, Code SC. ***The document may be retained.***

GENERAL AVAILABILITY

☐ Issue as a NASA Publication.

☒ May be made available without limitation (**Announce in STAR**).

N65 17609

☐ May be made available without limitation (**Not suitable for announcement in STAR e.g. status reports, administrative reports etc.**)

LIMITED AVAILABILITY

☐ **U. S. Government Agencies and Contractors Only.** (The document contains information that should be made available only to the U. S. Government and its Contractors.)

☒ **U. S. Government Agencies Only.** (The document should not be made available beyond Federal Agencies.)

☐ **NASA and NASA Contractors Only.** (The document should be made available only in support of a NASA contract.)

☐ **NASA Headquarters Offices and Research Centers Only.** (This document contains information that must not, at this time, be released outside NASA - Explain Below.)

PROGRESS ON THIS GRANT/CONTRACT IS: ☐ SATISFACTORY ☐ UNSATISFACTORY

REMARKS:

Winnie M. Morgan
Signature (~~Technical Monitor~~)

3-3-65
Date

FOR REPORTS CONTROL USE ONLY

NASA-TN Number CR 60905

NASA-TMX Number

(1)	(2)	(3)	(4)	(5)	(6)	(7)	(8)

1. For specified L-values in the range $2 \lesssim L \lesssim 7.5$ there is an apparent decrease in intensity of 40 keV and 230 keV electrons of about 2 to 3 orders of magnitude for $|B|$ going from ~ .2 to ~ .5 gauss.

2. The intensity of 1.6 MeV electrons also decreases ~ 2 orders of magnitude with $|B|$ going from ~ 0.2 to ~ 0.5 gauss and for $2 \lesssim L \lesssim 4.5$ the decrease in intensity due to the magnetic storm on June 6 is clearly evident.

Author

I. INTRODUCTION

The purpose of this study is to examine the morphology of the electron distribution in the outer zone from 237 to 2785 km by means of representative profiles of intensity versus L for various local times and by means of long term median intensities. The existence of an outer zone diurnal variation in electrons of energy > 40 keV for $L \gtrsim 8.0$ has been demonstrated previously in a gross manner [O'Brien, 1963; McDiarmid and Burrows, 1964a, b; Frank et al., 1964]; hence local time will be taken into account in this study. The present investigation will complement the prior work cited above by obtaining the morphology of the diurnal variation based on a collection of latitude profiles for both 40 keV and 230 keV electrons and by extending the gross study of the outer zone latitude and altitude dependence of electron fluxes.

II. COORDINATE SYSTEM

The coordinate system to be used is an L-local time system with McIlwain's /1961/ L parameter and geographic local time. The L-coordinate system is recognized to lose its simple geometrical interpretation in the outer zone ($L \gtrsim 3.0$); however L will be used in this study as an organizing parameter. Questions as to the physical significance of the L-coordinate system in the outer zone will be overlooked in this study, in view of the fact that at low altitudes L has proved to be the best parameter to date for organizing trapped particle intensities. L as used in this study is at least as valid as any other non-local time dependent parameter which is fixed to the earth because the data used were taken in a restricted range of longitude (~ 100°) at different local times /cf. Frank et al., 1964/.

III. DESCRIPTION OF THE EXPERIMENT

The overall design and details of the Injun III experiment are discussed elsewhere [O'Brien et al., 1964] and will not be given here. Only the design and characteristics of the pertinent detectors will be discussed.

The primary detectors to be used are the Anton type 213 Geiger-Mueller detectors designed and constructed by L. A. Frank and J. D. Craven of this laboratory. Two of the tubes used were thin-windowed (~ 1.2 mg/cm^2 mica) and sensitive to electrons of energy greater than ~ 40 keV and protons of energy greater than ~ 500 keV directionally. One of the 213 tubes (Detector 1) was oriented perpendicular to the B-vector (Injun III was magnetically oriented) with a conical collimator of half-angle 13°, the other (Detector 5), at 180° to the forward directed B-vector with a collimator half-angle of 43° (with declining efficiency as the angle from axial incidence increases). The directional geometric factors for the 90° detector and the 180° detector are $.65 \times 10^{-2}$ cm^2 sr and 5.5×10^{-2} cm^2 sr, respectively, for radiation which is isotropically distributed and filling the entire collimator. In this study the designation that detector 5 responds to pitch angles $\alpha < 43°$ and $\alpha = 0 \pm 43°$ are both used although negative pitch angles

are not strictly defined. The collimator of detector 5 is symmetrical about the B vector and the designation $\alpha = 0° \pm 43°$ designates this fact explicitly. The strictly correct designation for detector 5 is however $\alpha < 43°$. A 213 G.M. tube (Detector 3) was also placed at 90° to the B-vector with a collimator half angle of 13° giving a geometric factor of $\sim 2 \times 10^{-3}$ for electrons and shielded by a foil sufficient to raise the energy threshold to ~ 230 keV for electrons and ~ 4 MeV for protons. A 302 G.M. tube (Detector 6) which has only omnidirectional properties was also used with a geometric factor of approximately 0.75 cm^2 for direct counting and energy thresholds for direct counting of about 1.6 MeV for electrons and about 20 MeV for protons. There is an uncertainty in the effective energy thresholds and geometric factors for the G.M. tubes because both quantities depend strongly on the electron energy spectrum. Throughout this paper the nominal values of energy thresholds and geometric factors listed above will be used. The geometric factors are believed to be accurate to within a factor of 2. The effective energy thresholds for these detectors have been determined for various spectrums by J. D. Craven (Master's Thesis, 1964) using a numerical

integration and are shown in Table I (after Craven, 1964). $R(E, \gamma)$ is the product of the spectral form $j = j_o E^{-\gamma}$ ($J = J_o E^{-\gamma}$) (assumed) and the geometric factor and efficiency as a function of energy (both measured) and $X(E, \gamma)$ is the fraction of counts due to electrons above the energy E, for a spectrum characterized by γ.

IV. SELECTION OF REPRESENTATIVE LATITUDE PROFILES

One technique of studying the morphology of the outer zone in general and diurnal variations in particular is simply to examine the profile of the counting rate of a given detector versus L as the satellite traverses the outer zone at different local times. Since Injun III operated successfully for ten months and telemetry has been taken for some 1500 revolutions, i.e., passes through the outer zone at high latitudes, it is not practical to present such a quantity of latitude profiles as results. It is therefore necessary to select only certain passes for presentation as representative profiles, leaving the consideration of all passes to a statistical study which will supplement the results of Frank et al. [1964]. The selection of passes to be characterized as typical was designed to represent the outer zone in an unbiased way. In no case were passes discarded because of the properties of the counting rates. The first selection was made according to magnetic activity and data taken on the ten quietest days and five most disturbed days per month [Lincoln, 1963a, b, c, d] were used. Data from the months of April, May, June, and July, 1963, were used because the orbit during this period provided a good sampling of all local times. Only Northern Hemisphere data

were used because the precipitated electron detector looks the wrong direction along the field line in the Southern Hemisphere. The available passes in April, May, June, and July on quiet and disturbed days were tabulated and approximately half of these were rejected because the data were not acquired for the entire pass from L = 4 to L = 8 with breaks of no more than 1.0 in L. The remaining passes were then classified according to local time and from each of four classifications according to local time 10 quiet day passes and 5 disturbed day passes were randomly selected. A tabulation of the passes selected is given in Table II.

V. TREATMENT OF DATA IN THE STATISTICAL REPRESENTATION OF THE OUTER ZONE FOR JANUARY, FEBRUARY, MARCH, APRIL, MAY, JUNE, JULY, AND SEPTEMBER, 1963

The Injun III data output was routinely summed into 8-second count accumulations and merged with the orbit parameters B, L, and local time. A smoothing criterion was then applied to eliminate noisy data. A check of the output of the application of smoothing criterion by comparison with the input yielded the result that ~ 20% to 30% of the data points were randomly eliminated and all but ~ 5% of the spurious points were eliminated. The remaining questionable data points do not affect the medians significantly. The data were then sorted into several categories specified by selected ranges of the parameters L, B, and local time. L ranges of 0.50 and B ranges of 0.20 gauss were generally used. On each revolution the satellite crossed a given L shell at a given B-value (altitude) only once at a given local time. Occasionally more than one data point was obtained per crossing of a given B-L range, but these cases were easily identified and only one data point was used; hence each distinct traversal of a given range in B and L has equal weight.

VI. REMARKS ON B-DEPENDENCE

Because of the eccentricity of the Injun III orbit the value of scalar B at the satellite for a given L-shell varied by about a factor of 2.5 for most L values, e.g., from B = 0.19 to .53 gauss for L = 4.5. The variation of B at the satellite caused the detectors which respond to a fixed range of pitch angles to sample various intervals of the equatorial pitch angle distribution as the line of apsides precessed in the orbital plane. If the equatorial pitch angle distribution is, on the average, not isotropic in the range of pitch angles which would be counted by Injun III detectors, then the counting rates would be, on the average, different for different values of B at the satellite.

Plots were made of the counting rates of each detector as a function of B at the satellite for specific L-shells, examples of which are shown in Figures 4 to 6, 13 to 15, 21 to 23, and 26 to 30 which will be discussed in more detail in succeeding sections. The L-intervals used were: 2.0 ± 0.1, 2.2 ± 0.1, 2.3 ± 0.1, 2.6 ± 0.1, 2.8 ± 0.1, 3.0 ± 1, 3.5 ± 0.25, 4.0 ± 0.25, 4.5 ± 0.25, 5.0 ± 0.25, 5.5 ± 0.25, 6.0 ± 0.25, 6.5 ± 0.25, 7.0 ± 0.25, and 7.5 ± 0.25. These plots proved to be successful in organizing the data to a degree which generally decreased as L increased.

Medians were taken at 0.20 gauss intervals and then fit graphically with a curve or line. No attempt was made to account for real temporal variations except for the classification of detector 6 counting rates into two epochs in real time. Real temporal variations are presumably a significant cause of the scatter which is seen in the intensity versus B plots, e.g., Figures 4 to 6, 13 to 15, 21 to 23, and 26 to 30. At $L \sim 2.0$ the typical range of intensity at a given B-value is a factor of 2 or 3 and at $L \sim 7.0$ about 2 orders of magnitude.

The B-dependence ranges from reasonably clear at $L \lesssim 2.0$, i.e., there is much less scatter of intensities (factor of 2 or 3) at a given B value than the total apparent variation (3 to 4 orders of magnitude) of intensity with B, to very uncertain at $L \sim 6.0$ to 7.5 where the typical range of intensity for a given L and specific B value is 2 orders of magnitude as compared to an apparent variation of the medians with B of about two orders of magnitude or less. Hence, insofar as the scatter of the data reflects the certainty with which a B dependence can be established, that B dependence shown for the higher L-values ($L \sim 6.0$ to 7.5) is generally less certain than that for lower L-values. The reliability of such plots of I_{median} vs B for

specific L values can be checked by examining in detail cases for which two crossings of an L shell separated by a brief interval in real time are available during which intensities in the outer zone are shown to be time stationary. This will be done in a later section.

VII. THE MORPHOLOGY OF THE OUTER ZONE AT LOW ALTITUDES AS A FUNCTION OF LOCAL TIME

A. Electrons of Energy $E_e \geq 40$ keV at Large Pitch Angles ("Trapped")

The representative latitude profiles of trapped 40 keV electrons are shown in Figures 1 and 2 and the following remarks are made. In the L-range from about 8 to 16 a 2 to 3 order of magnitude enhancement of intensity is observed starting in the morning hours and lasting through mid-day which agrees qualitatively with prior observations [O'Brien, 1963; Frank et al., 1964; McDiarmid et al., 1964a]. The nighttime profiles are usually characterized by a sharp and well defined decrease in intensity at about $L \sim 8.0$ which is usually taken to indicate the sensible limit of durable trapping of 40 keV electrons. The relationship between the limit of durable trapping of 40 keV electrons at high latitudes and the magnetospheric boundary [cf. Freeman, 1963] observed in the equatorial plane is not clear. In no case from about 09:00 to about 15:00 local time was a sharp decrease in intensity of 40 keV electrons observed--in contrast to local night when a sharp decrease was commonly observed. The dawn and evening profiles are transitional, and the general form of the profiles is more

variable, lying between night-like and day-like forms. No diurnal effect for $4 \leq L \leq 8$ is evident in the representative profiles. In summary of the observations of latitude profiles, the large enhancement of trapped electrons $8 \leq L \leq 16$ during local day is the most dominant effect in both quiet and disturbed times.

The median latitude profiles of trapped 40 keV electrons are shown in Figure 3 where local time intervals of 6 hours were used corresponding to dawn, midday, evening, and midnight. For $L \leq 7.5$ an empirical B-correction of the median for different local times has also been made so the corrected profiles can be taken to represent cuts through the outer zone at constant B. The diurnal variation of the high-latitude boundary is clearly evident in the corrected medians. If 1% of the outer zone "plateau" flux is taken as the boundary, the boundary occurs at $\Lambda = 72°$, $75°$, $74°$, and $69.5°$ for dawn, midday, evening, and midnight, respectively. The procedure for correction for B-dependence is outlined in Appendix I. For $\Lambda \leq 65°$ no appreciable diurnal variation of trapped 40 keV electrons is observed. The only indication of the presence of a "slot" in 40 keV electrons is the small (factor of 2 to 5) decrease which occurs at about $\Lambda = 57°$ or $58°$ for all local time as contrasted to the 2 order of magnitude "slot" for the

230 keV and 1.6 MeV electrons at $\lambda \simeq 55°$ for all local times (cf. Figure 20).

The typical B-dependence of trapped 40 keV electrons is illustrated in Figures 4, 5, and 6 which are characteristic of the entire group of such plots which were used to correct the median latitude profiles. At L = 2.2 and 2.6 in Figure 4 there is clearly a decrease by factors of 300 and 30, respectively, in intensity as B goes from .18 to .42, an increase of about a factor of 2.4. The equatorial pitch angles of these particles are in the range 0° to 2° or 3°, hence it may be inferred that at the equator the directional intensity increases by about one or two orders of magnitude in the first several degrees away from 0° for L = 2.2 and 2.6. These plots of $j\ (90°)$ vs B allow the evaluation of the median $\frac{\partial j}{\partial j_o}$ for $0 \leq \alpha_o \leq \sim 3°$, a quantity which would otherwise be quite difficult to observe. At L = 3.5 and 4.5 as seen in Figure 5 the decrease in intensity is by factors of 50 and 20, respectively, as B increases from .20 to .50, a factor of 2.5. For these L values more scatter is evident than at L = 2.2 and 2.6; however both the median and the envelope of the data show consistent decreases with increasing B and one may still be reasonably certain that the tendency is for a

decrease in intensity with increasing B at a rate given approximately by that quoted above. At L = 6.0 and 7.0 as illustrated in Figure 6 the scatter of intensities becomes quite large. This fact is presumably a result of large real time variations as well as local time variations starting at L ~ 7.0. The medians tend to decrease about one order of magnitude in intensity as B goes from 0.20 to 0.52 gauss, a tendency which is consistent with behavior seen at lower L-values. The claims which are made for the B-dependence especially for $L \geq 6.5$ must be prefaced by an uncertainty because of the large scatter of intensities. The obscuration of any B dependence at high L values is also consistent with the observation at low L values that the B dependence becomes generally weaker with increasing L. The summary of the median B dependence of 40 keV trapped electron intensities is shown in Figures 7 and 8.

B. Electrons of Energy $E \geq 40$ keV at Small Pitch Angles

The representative profiles of the intensity of 40 keV electrons at small pitch angles ($\alpha < 43°$) are illustrated in Figures 9, 10, and 11. The counting rates are characteristically erratic, especially in the range $L \gtrsim 8.0$ because of large variations of electron intensity in times on the order of seconds and in distances of tens of kilometers. Such rapid

fluctuation of intensity has been found to be characteristic of electrons at small pitch angles in the outer zone in previous studies [O'Brien, 1962, 1964]. The primary objectives of this study are to examine the B, L, and local time dependence of precipitated 40 keV electrons [cf. Frank et al., 1964; McDiarmid and Burrows, 1964a, b], and insofar as the erratic fluctuations do not obscure the general trend of the data as a function of B, L, and local time, such fluctuations will be ignored.

The counting rate of detector 5 has been converted to an equivalent directional intensity of electrons for an isotropic beam of electrons incident on the detector. The directional intensity of electrons is very probably not constant over all pitch angles less than 43°, hence the counting rate represents an average over the anisotropic distribution weighted by the efficiency of the detector as a function of angle from axial incidence. The equivalent intensity is used in order to facilitate comparison with other detector counting rates but it must be noted that the directional intensity quoted represents a weighted average over the real angular distribution.

The profiles of the directional intensity of electrons $E_e \geq 40$ keV at small pitch angles ($\alpha < 43°$) usually

represent particles which are precipitated and lost into the atmosphere. For purposes of this study all particles mirroring below 100 km are presumed to be lost in the atmosphere. This distinction is clearly approximate because the loss cone is not sharp. However it is a reasonable criterion to use since Injun III did not measure the backscattered particles simultaneously with the precipitated particles in order to experimentally define the loss cone. In terms of this study the criterion for Detector 5 ($\alpha \leq 43°$) to measure only precipitated particles becomes that $\alpha = \sin^{-1} B/B_{100} \leq 43°$ from the Alfven approximation, $B_{100} = B$ at 100 km altitude for the satellite L and longitude, and α is the half angle of the cone of precipitated particles. Or in other terms, the acceptable value of B at the satellite for Detector 5 to measure only particles mirroring below 100 km is $B \geq B_{100} \sin^2 43°$. This criterion was then tested at L = 4,5,6,7,8,10,12 and the passes for which the test failed are indicated by dotted lines in Figures 9, 10, and 11. Therefore, the portions of the curves of Figures 9, 10, and 11 which are not dotted can be taken to represent particles mirroring at or below 100 km.

Although the representative profiles of the intensity of small pitch angle 40 keV electrons are typically quite irregular,

occasionally fluctuating abruptly by as much as two orders of magnitude, certain general features may be distinguished which are worthy of comment. The first and most prominent feature which can be seen in both quiet (Figures 9 and 10) and disturbed (Figure 11) times is the marked diminution of intensity for $L \geq 8$ during local night, 21:00 to 03:00 as compared to those for local day 09:00 to 15:00. Electron intensities for $L \gtrsim 8$ seem to be about 2 orders of magnitude less during local night than local day, a result which is in agreement with observations of Frank et al. [1964] and McDiarmid et al. [1964a] and which is further corroborated by statistical results of this study. Another observation which arises from the study of the representative profiles is that of the abruptness (e.g., decrease by 2 orders of magnitude within 1.0 interval of L) of the high latitude termination of precipitated electron intensities around midnight as compared to that around local noon. The high latitude termination was never observed to be abrupt during 09:00 to 15:00 and was observed to be abrupt in at least 80% of the time during 21:00 to 03:00 in these profiles.

A curious feature which is commonly seen in the quiet time profiles from about 21:00 to 05:00 is an enhancement

(typically a factor of 5) of 40 keV electron intensity over a narrow range in L (~ 0.5) in the region $6.0 \leq L \leq 10.0$ usually associated with a sharp decrease in intensity to higher L values. Out of 19 eligible passes such a sharp enhancement was observed 13 times or in about 68% of the cases. Because of the sharp character of such an enhancement on its movement in latitude from pass to pass, it would not be evident in a study of median or average intensities and must be observed in a pass by pass study such as done here. This observation is in general agreement with results of O'Brien [1962, 1964] that precipitation of 40 keV electrons is generally enhanced near the high latitude termination. However we would add the remark that such enhancement seems to be most evident in quiet times and in the local time range from about 21:00 to 05:00.

The median latitude profiles of 40 keV electrons at small pitch angles are shown in Figure 12. In order to assure that these profiles would be characteristic of precipitated electrons, all data points which were included were taken at B values equal to or exceeding 0.27 gauss which insured that Detector 5 was responding to electrons mirroring at or below 100 km for all the L values used. The median profiles were corrected for $L \leq 7.5$ to a constant value of B = 0.30 gauss

from the empirically derived B dependence as seen in Figures 13, 14, 15, 16, and 17. The correction procedure is described in Appendix I. The diurnal variation is seen quite clearly in the median profiles of precipitated 40 keV electrons for $\Lambda \geq 65°$ where the median intensity during the night (21:00 to 03:00) and dawn (03:00 to 09:00) starts to decrease rapidly and drops by two orders of magnitude between 65° and 70° while during midday (09:00 to 15:00) and evening (15:00 to 21:00) the decline is by factors of 2 and 4, respectively. The highest median value of precipitated 40 keV electron intensity in the outer zone was found to be $\sim 2 \times 10^4$ $(cm^2 \text{ sec sr})^{-1}$ during local midday in the range $\Lambda = 60°$ to 65° (L = 4 to 5.5). There is in the medians a dawn-evening asymmetry for $\Lambda \geq 70°$ with the dawn median profile strongly resembling that for midnight and the evening profile resembling that for midday. At $\Lambda = 70°$, for example, the median intensity is about 10^3 $(cm^2 \text{ sec sr})^{-1}$ for evening and about 2×10^2 $(cm^2 \text{ sec sr})^{-1}$ for dawn. Although the evening median points are irregular, every one for $\Lambda \geq 70°$ is higher than its corresponding dawn median.

The B-dependence of 40 keV electrons at small pitch angles $\alpha < 43°$ is shown in Figures 13, 14, 15, 16, and 17.

At L = 2.2 and 2.6, Figure 13, the medians decrease by factors of ~ 1200 and ~ 500, respectively, as B increases by a factor of 2 from 0.20 to 0.40 gauss. The typical range of intensities at a given B value is a factor of 2 to 6. The B dependence is quite clear at these L-values. Part of the increase scatter at low intensities ($\lesssim 2 \times 10^2$) is due to the statistical uncertainty of low counting rates. At L = 3.5 and 4.5 shown in Figure 14 the scatter of intensities increases to about 1 to 2 orders of magnitude at a given B value which is comparable to the total variation of the medians. The observations which can be made regarding the B dependence from these plots are necessarily uncertain because of the scatter. The general shape of the variation of the medians with B is comparable to that seen at L = 2.2 and 2.6, where the variation is much more distinct. The medians tend to follow the general envelope of the data and the small fluctuations in the medians are considered to be insignificant in the presence of such large scatter, thus a straight line fit of the medians was chosen as an approximate representation of the B dependence. At L = 5.5, Figure 15, the scatter at a given B value is generally one order of magnitude, except for B $\gtrsim$ 0.38 where two orders of magnitude is more characteristic. Here again the behavior

of the medians is generally consistent with the envelope and with the variation observed at lower L-values. At L = 7.0, Figure 15, the scatter is about 2 to 3 orders of magnitude and the apparent B variation about 2 orders of magnitude; hence the B variations is very uncertain. This plot is included for completeness and the medians can be fit with an approximate straight line which is not inconsistent with the general pattern of observed B dependence. Both real and local time variations have become quite large at L = 7.0.

C. Electrons of Energy Greater Than 230 keV at Large Pitch Angles ($\alpha = 90° \pm 13°$)

The representative latitude profiles of the directional intensity of 230 keV electrons are shown in Figures 18 and 19. The profiles of 230 keV electrons are very smooth in comparison with those for 40 keV electrons, on both quiet and disturbed days, and typically have an outer zone maximum in intensity at about L = 4.5 to 5.5 and a regular decrease at higher L-values to the threshold of the counter for $L \geq 7.0$ to 8.0. A slight enhancement of intensity is noted near local noon in the L range 5.5 to 7.0 which appears as a slower rate of decrease of intensity for increasing L. The pass to pass variations in intensity appear to be more prominent in the disturbed day profiles than in the quiet day profiles.

The median profiles are shown in Figure 20 for dawn, midday, evening, and midnight of the directional intensity of 230 keV electrons corrected to B = 0.30 gauss as outlined in Appendix I using the empirically derived B dependence shown in Figures 21, 22, and 23, and in summary in Figures 24 and 25. The most prominent feature of the profiles is the low value of intensity of 230 keV electrons in the region of $\wedge \cong 55° \pm 2.5°$ ($L \cong 3.0 \pm 0.5$) at all local times. When the 230 keV profiles are compared to those for 40 keV by computing ratios of median intensity of 40 keV to that of 230 keV as seen in Table III, it becomes evident that the integral spectrum becomes softer as L increases towards 3.0 ($\wedge = 55°$) and then harder again as L goes to 4.5 ($\wedge \cong 62.5°$) and then softer again for $L \geq 4.5$. There is also a small diurnal effect in the median profiles which can be seen by considering the median intensities at $\wedge = 67.5°$ which are 2.5×10^4, 5.0×10^3, 1.3×10^3, and 9.0×10^3 for midday, evening, midnight, and dawn, respectively. This slight enhancement of 230 keV electron intensity around midday is also observed in the representative profiles.

The B dependence of 230 keV electron directional intensity at $90° \pm 13°$ is shown in Figures 21, 22, and 23, and in summary

in Figures 24 and 25. At L = 2.2 in Figure 21, the median intensity is seen to decrease by about 2 orders of magnitude as B increased from 0.16 to 0.38 gauss, where the intensity generally went below the sensitivity of the counter. The scatter of intensity at a given B value was comparatively small, generally factors of about 3 to 10. At L = 2.6 the intensities were generally near the threshold of the counter and statistical fluctuations are more severe because of the low counting rate. The general shape of the medians is a decrease with increasing B. At L = 3.5 in Figure 22 the scatter of intensities is quite severe, commonly 2 orders of magnitude and the total apparent variation of the medians is about 1 order of magnitude, hence the conclusions which may be drawn from this plot are restricted. The large scatter of intensities at this L value, 3.5, is consistent with the observation that L = 3.5 is in the region where the intensity increases rapidly towards the outer zone maximum and a small excursion in L of the maximum intensity could easily produce such scatter of intensities at L = 3.5.

At L = 4.5 the B dependence as seen in Figure 22 is more certain than at 3.5 because the scatter at a given B value is less than 1 order of magnitude and the total apparent

variation of the medians is about a factor of 30 and the envelope of the data also resembles quite closely the variation of the medians. The B dependence of 230 keV electrons for L = 6.0 is shown in Figure 23, along with that for 7.0. For L = 6.0 the scatter is severe and it will only be claimed that the median generally tends to decrease with increasing B, a fact which is consistent with the more distinct and certain dependence seen at lower L values. The plot for L = 7.0 is included for completeness and is not intended to show a clear B dependence and is not claimed as such. The summary of median curves of directional intensity of trapped 230 keV electrons for $2.0 \leq L \leq 7.0$ are shown in Figures 24 and 25.

D. Electrons of Energy Greater Than 1.6 MeV, Omnidirectional

Representative profiles were derived for the omnidirectional intensity of electrons just as for the 40 keV and 230 keV electrons; however since no appreciable diurnal effect in the intensity was detected in the presence of large variations in real time, the representative profiles will be omitted in favor of an extended study of the B dependence. The reason for the inclusion of a more detailed study of the B dependence of the

omnidirectional intensity of 1.6 MeV electrons is an apparent decrease in intensity which occurred between revolutions 2197 and 2201 or, in universal time, between ~ 19:39:34 on June 7 and ~ 02:44:46 on June 8. This temporal change reduced the intensity of 1.6 MeV electrons by a factor of 10 or more for $2.0 \lesssim L \lesssim 6.5$ to the threshold of the 302 counter. The intensity remained at the threshold of the counter for $L \gtrsim 2.0$ until revolution 2203, 06:28:53, June 8, when the intensity was found to have begun to recover, especially in the range $L \gtrsim 3.5$. The intensity for $2.0 \lesssim L \lesssim 4.5$ remained low for the remainder of June and July, as can be seen in the plots of intensity versus B in which the intensities are separated into before and after revolution 2200 (Figures 26 to 29). For $L > 4.5$ the intensity recovered within a few passes. The decrease in intensity of 1.6 MeV electrons in the outer zone on June 8, 1963 occurred in the recovery phase of a gradual commencement magnetic storm which began about 14:00 to 17:30 UT on June 6. K_p reached 7 for 00:00 to 03:00 on June 7 [Lincoln, 1963a, d; 1964a, b]. All magnetic observatories reported in the Journal of Geophysical Research recorded the storm.

Considering first L = 2.0 and 2.2 as shown in Figure 26 where the data points from revolutions prior to 2200 are indicated by the open symbols and those from revolutions after 2200 by filled symbols. At L = 2.0 the total variation of the medians is about 3 orders of magnitude decrease as B increases from .16 to .30 gauss and the intensities scatter over less than one order of magnitude at a given B value, especially when the data are separated according to before or after revolution 2200. The B dependence is fairly distinct at L = 2.0 and the separation of the median intensity versus B plot into two groups, the two real time groups, is becoming evident. At L = 2.2 the B dependence is very clear and the temporal change of the intensity versus B plot is apparently larger and more distinct than at L = 2.0. The typical temporal change in median intensity is about a factor of 3 to 10. A clear B dependence and a distinct separation of the curves for before and after the temporal variation is observed to persist through L = 2.4 and 2.6 (Figure 27), L = 2.8 and 3.0 (Figure 28). At L = 3.5 and 4.5 (Figure 29) the intensities are scattered over 1 to 2 orders of magnitude for a specific B value and the intensities are not clearly separated in the temporal classification; hence the B dependence as derived

from the median intensities is less certain. The apparent decrease in the median intensity at L = 3.5 and 4.5 for revolutions prior to 2200 is about 3 and 2 orders of magnitude, respectively, as B increases from 0.20 to 0.50 gauss. The general envelope of the data and the trend to the medians indicate a B dependence consistent with that seen at the lower L values. The 3 order of magnitude scatter of intensities is very serious at L = 6.0 as shown in Figure 30 as compared to the apparent 2 order of magnitude variation of the medians. Very little can be concluded from such a plot. The general trend of the medians is not inconsistent with the variation seen at lower L values. Also in Figure 30 it may be seen that at L = 7.0 the intensity of 1.6 MeV electrons generally stays near the threshold of the counter and the study must be terminated in L. A summary of only the medians of omnidirectional intensity of 1.6 MeV electrons and the graphically established best curves for all L values in the range $4.5 \leq L \leq 6.5$ is shown in Figure 31.

The overall latitude profile as seen in Figure 32 for the omnidirectional intensity of 1.6 MeV electrons is represented by the intersection of the intensity versus B curves with the line B = constant, which in this case was B = 0.30 gauss. For $45° \leq \lambda \leq 60°$ two separate intensity versus B curves

were necessary for before and after revolution 2200; hence two separate latitude profiles were derived. For $\lambda \geq 65°$ there was no distinct separation of the data points according to real time and all the data were grouped together in order to finish the profile. The overall profile for the 1.6 MeV electrons is similar to that for 230 keV electrons except for the real time variation present in the 1.6 MeV profile.

E. Detailed Study of Several Passes

A good test of the validity of the B-dependence of outer zone electron intensities which is claimed in this paper is provided by those portions of the satellite data for which there are several intersections of the same L shell at different B values separated in real time by only a few tens of minutes, especially in those instances where it may reasonably be concluded that the intensities are approximately constant in real time and in longitude and local time. When the intensities appear to be constant, the observation of an intensity at a given B, L value should allow the prediction of the intensity at the next intersection of the same L shell at another B value, an example of which is Revolution 2022 as shown in Figure 33. For values of $L \leq 3.0$ the prediction could not be tested because suitable data were not obtained. For Detector 1,

40 keV electrons at $\alpha = 90° \pm 13°$ the largest discrepancy between the predicted and observed intensity is about 30% at L = 4.5. Detector 5 readings which measure 40 keV electrons at $\alpha = 0° \pm 43°$ were predicted to within a factor of 2. The predictions for Detector 3 which responded to 230 keV electrons at $\alpha = 90° \pm 13°$ were correct to within 30% or 40%, except at L = 3.5, which deviated by a factor of 1.8. The larger deviation for Detector 3 at L = 3.5 is not surprising in view of the larger scatter, hence greater uncertainty at L = 3.5 than at other L-values. The deviation of the predicted and observed intensities of 1.6 MeV electrons is less than 50% for all L values tested except at L = 3.5 where the discrepancy was by a factor of about 3.6, which was almost the total observed difference in intensity. There are times when the electron intensities in the outer zone are clearly not time stationary (real or local time) over the 15 to 50 minute real or 3 to 10 hour local time span which the satellite requires to recross a given L shell. Revolution 1886 as shown in Figure 34 was such an obviously non-time stationary situation. The predicted intensities are greatly in error and for each detector the intensity profiles intersect between L = 5.5 and 6.0 although the B values are different by about 0.10 gauss.

Unless one claims that there is no dependence of intensity on B, i.e., isotropic equatorial pitch angle distribution for $\alpha_o \leq 2°$ or $3°$ one must conclude that the intensity is indeed time varying and an overall B dependence would not be expected in itself to explain the observed difference in intensities.

VIII. SUMMARY OF RESULTS

The results of the study discussed above may be listed very briefly as:

(1) There is a 2 to 3 order of magnitude daytime enhancement of both trapped and precipitated 40 keV electrons in the range $8.0 \lesssim L \lesssim 16$ which persists in both quiet and disturbed periods.

(2) There is a strong tendency for a sharp, narrow enhancement in precipitated 40 keV electrons during local night (21:00 to 05:00) which occurs 0.2 to 0.3 L-value less than the high latitude termination of trapping. This enhancement is most prominent in quiet times.

(3) The decrease in intensity of 40 keV electrons to higher L-values for $L \geq 6$ to 8 is invariably much more gradual during local day than local night.

(4) There is apparently a slight enhancement ($\sim$ 1 order of magnitude) of trapped 230 keV electrons during local day for $5.5 \lesssim L \leq 7.0$, otherwise the profiles are quite regular as a function of local time.

(5) There is no apparent large local time effect in the omnidirectional intensity of electrons $E_e \gtrsim 1.6$ MeV as determined from the collection of individual profiles.

(6) There was a decrease of about 1 order of magnitude in the omnidirectional intensity of 1.6 MeV electrons on June 7 to 8, 1963 for $2.0 \leq L \leq 4.0$ preceded and followed by periods on the order of one month of relatively stable intensity.

(7) The gross dependence of the median intensity of 40, 230, and 1600 keV electrons on B in the outer zone has been derived generally with decreasing clarity as L increases.

IX. DISCUSSION AND INTERPRETATION OF RESULTS

The diurnal variation in trapped 40 keV electrons in the outer zone found in this study is in agreement with results obtained by O'Brien [1963], McDiarmid and Burrows [1964a], and Frank et al. [1964]. The variation of precipitated 40 keV electrons is similar to that reported by McDiarmid and Burrows [1964a] and Frank et al. [1964]. The diurnal variation in 230 keV electrons obtained from Injun III is very similar to that observed by Williams and Palmer [1964] for 280 keV electrons. Williams and Palmer find that the diurnal variation of 280 keV electrons can be explained simply by considering the drift paths which conserve μ and I for such particles in the distorted magnetosphere. The explanation of diurnal effects observed in the distribution of 40 keV electrons, both precipitated and trapped clearly requires detailed consideration of the motion of such particles in the highly distorted portion of the magnetosphere for $L \geq 8.0$. Electric fields in the magnetosphere affect the motion of 40 keV electrons significantly [cf. Hones, 1963]. The experimental determination of the properties of the geomagnetic field at large radial distances [cf. Cahill and Amazeen, 1963; Cahill, 1964; Ness et al., 1964] combined with the theoretical computation of electron motions in such fields will greatly aid in the understanding of the

diurnal variation. The observation of the energy dependence of the diurnal variation, especially for electron energies less than 40 keV is also of interest.

The temporal variation in 1.6 MeV electrons which was observed on June 7 and 8, 1963 is similar to other such occurrences [Pizzella et al., 1962; Forbush et al., 1962]. A notable feature of the decrease was that it was preceded and followed by periods of over one month during which the intensity variation was relatively small, hence the B dependence of intensity was determined for both the period preceding and following the decrease. The decrease in intensity of 1.6 MeV electrons was apparently produced by a gradual commencing $K_p = 7$ magnetic storm on June 6.

APPENDIX I

Method of Correction of Medians to a Constant Value of B

In order to reliably compare the median latitude profiles of electron intensity as a function of local time account must be taken of B dependence because the local time of a data sample is related to the B value through the properties of the orbit. The gross B dependence was examined at each L value by plotting intensity vs B for all the data and by taking medians on 0.2 gauss intervals. A simple curve was then graphically fit to the medians as shown in Figures 7, 8, 16, 17, 24, 25, and 31. For some L values the temporal scatter of the intensities was small and the medians were easily fit with a simple curve and one could be reasonably sure of the B dependence. For other L-values, notably the higher ones, the scatter of the data was quite large and the corresponding results for B dependence were less certain. The range of L values for which the B dependence was found to be sufficiently certain for a correction to be used were:

Detector 1	$2.0 \leq L \leq 7.5$
Detector 3	$2.0 \leq L \leq 6.5$
Detector 5	$2.0 \leq L \leq 7.5$
Detector 6	$2.0 \leq L \leq 6.0$

After the B dependence of the median intensity was established the median intensities were corrected to a constant value of B = 0.30 gauss by graphically subtracting from or adding to the logarithm of a given intensity reading an amount which was the logarithm of the intensity difference between the median intensity curve at the B value for a given point and for 0.30 gauss. The median of the corrected data points was then taken. Exactly this procedure was followed for all local times and L values for which there were 20 or less data points and for any situation where the data were not distributed uniformly in B. In most cases the median intensity itself as a function of L and local time was corrected using as the difference in B the difference between the median B value of the L-local time group and B = .30 gauss. The difference between the result of correcting the median intensity and the median of the corrected intensities was only a few percent where both types of correction were tested in situations where there were 20 or more data points evenly distributed in B.

ACKNOWLEDGEMENTS

The author wishes to express his thanks to Professor J. A. Van Allen whose advice and encouragement made this study possible and to Dr. L. A. Frank who provided many valuable suggestions as well as implementation of data reduction programs used in this study. We thank Dr. E. W. Hones for helpful discussions of our findings. We must also thank Dr. B. J. O'Brien, Mr. C. D. Laughlin, and Mr. D. A. Gurnett who successfully designed and executed Injun III experiment. Fabrication and calibration of detectors used in this study was done by Dr. L. A. Frank and Mr. J. D. Craven. We are also indebted to all of the individuals involved in the Injun III data reduction effort, in particular to B. Brechwald, D. Strottman, and B. Thomas.

REFERENCES

Cahill, L. J., Preliminary results of magnetic field measurements in the tail of the geomagnetic cavity, Trans. AGU, 45, 231-235, 1964.

Cahill, L. J., and P. G. Amazeen, The boundary of the geomagnetic field, J. Geophys. Res., 68, 1835-1843, 1963.

Craven, J. D., The temporal variations of electrons at low altitudes in the outer radiation zone as observed with satellite Injun III, Master's Thesis, University of Iowa, 1964.

Frank, L. A., J. A. Van Allen, and J. D. Craven, Large diurnal variations of geomagnetically trapped and of precipitated electrons observed at low altitudes, J. Geophys. Res., 69, 3155-3167, 1964.

Forbush, S. E., G. Pizzella, and D. Venkatesan, The morphology and temporal variations of the Van Allen radiation belt, October 1959 to December 1960, J. Geophys. Res., 67, 3651-3668, 1962.

Freeman, J. W., The morphology of the electron distribution in the outer radiation zone and near the magnetospheric boundary as observed by Explorer XII, J. Geophys. Res., 69, 1691-1723, 1964.

Hones, E. W., Jr., Motions of charged particles trapped in the earth's magnetosphere, J. Geophys. Res., 68, 1209-1219, 1963.

Lincoln, J. V., Selected geomagnetic and solar data, J. Geophys. Res., 68, 4862, 1963a.

Lincoln, J. V., Selected geomagnetic and solar data, J. Geophys. Res., 68, 5307, 1963b.

Lincoln, J. V., Geomagnetic and solar data, J. Geophys. Res., 68, 5879-5882, 1963c.

Lincoln, J. V., Geomagnetic and solar data, J. Geophys. Res., 68, 6199-6200, 1963d.

Lincoln, J. V., Geomagnetic and solar data, J. Geophys. Res., 69, 525-528, 1964a.

Lincoln, J. V., Geomagnetic and solar data, J. Geophys. Res., 69, 5087, 1964b.

McDiarmid, I. B., and J. R. Burrows, High latitude boundary of the outer radiation zone at 1000 km, Can.J. Phys., 42, 616-627, 1964a.

McDiarmid, I. B., and J. R. Burrows, Diurnal intensity variation in the outer radiation zone at 1000 km, to be published in Can. J. Phys., 1964b.

McIlwain, C. E., Coordinates for mapping the distribution of magnetically trapped particles, J. Geophys. Res., 66, 3681-3691, 1961.

Ness, N. F., C. S. Scearce, and J. B. Seek, Initial results of the IMP I magnetic field experiment, J. Geophys. Res., 69, 3531-3569, 1964.

O'Brien, B. J., Lifetimes of outer zone electrons and their precipitation into the atmosphere, J. Geophys. Res., 67, 3687-3706, 1962.

O'Brien, B. J., A large diurnal variation of the geomagnetically trapped radiation, J. Geophys. Res., 68, 989-995, 1963.

O'Brien, B. J., High latitude geophysical studies with satellite Injun 3. Part 3. Precipitation of electrons into the atmosphere, J. Geophys. Res., 69, 13-45, 1964.

O'Brien, B. J., C. D. Laughlin, and D. A. Gurnett, High latitude geophysical studies with satellite Injun 3. Part 1: Description of the satellite, J. Geophys. Res., 69, 1-12, 1964.

Pizzella, G., C. E. McIlwain, and J. A. Van Allen, Time variations of intensity in the earth's inner radiation zone, October 1959 through December 1960, J. Geophys. Res., 67, 1235-1253, 1962.

Williams, D. J., and W. F. Palmer, Distortions in the radiation cavity as measured by an 1100 km polar orbiting satellite, Johns Hopkins University Preprint, 28 August 1964.

TABLE I

(after Craven, 1964)

The Quantity $X(E, \gamma) = \dfrac{\int_{E}^{\infty} R(E, \gamma)\, dE}{\int_{0}^{\infty} R(E, \gamma)\, dE} \times 100\%$ for Several Injun III G.M. Tubes

X (γ, E)	Detector Designation	Electron Energy (MeV)					
		γ = 1	γ = 2	γ = 3	γ = 4	γ = 5	γ = 6
100%	*213A-213D	0.03	0.03	0.03	0.03	0.03	0.03
	213B	0.4	0.4	0.4	0.3	0.01	0.01
	302	3	2	2	0.07	0.02	0.02
90%	213A-213D	0.06	0.05	0.04	0.04	0.04	0.035
	213B	0.8	0.6	0.5	0.4	0.04	0.02
	302	5	3	2.5	0.2	0.05	0.05
70%	213A-213D	0.2	0.07	0.05	0.05	0.045	0.045
	213B	1	0.9	0.65	0.6	0.4	0.025
	302	11	5	3	2.5	0.07	0.06
50%	213A-213D	0.6	0.1	0.06	0.06	0.055	0.05
	213B	2	1	0.8	0.7	0.6	0.035
	302	22	7	4	3	0.09	0.07
30%	213A-213D	2	0.2	0.08	0.07	0.055	0.055
	213B	5	2	1	0.9	0.7	0.06
	302	43	12	6	4.5	0.12	0.08

TABLE I
(continued)

X (γ, E)	Detector Designation	Electron Energy (MeV)					
		$\gamma = 1$	$\gamma = 2$	$\gamma = 3$	$\gamma = 4$	$\gamma = 5$	$\gamma = 6$
10%	213A-213D	6	0.5	0.17	0.09	0.08	0.07
	213B	8	5	2	1.5	1	0.5
	302	76	26	9	6.5	0.3	0.13

*213A corresponds to Detector 1
213D corresponds to Detector 5
213B corresponds to Detector 3
302 corresponds to Detector 6

TABLE II

Distribution of Passes Selected for Typical Latitude Profiles*

Quiet												
Group 1			Group 2			Group 3			Group 4			
Rev. No.	Mo.	Day	Rev. No.	Mo.	Day	Rev. No.	Mo.	Day	Rev. No.	Mo.	Day	
1948	5	18	1997	5	22	2242	6	11	2716	7	19	
1961	5	19	1959	5	19	2266	6	13	2665	7	15	
2022	5	24	1919	5	16	2506	7	2	2652	7	14	
1800	5	7	1943	5	18	2656	7	14	2651	7	14	
2159	6	4	2668	7	15	2668	7	15	1638	4	24	
1811	5	7	2156	6	4	2655	7	14	1688	4	28	
2233	6	10	2308	6	16	2667	7	15	1699	4	28	
1948	5	18	2270	6	13	2641	7	13	1700	4	29	
1910	5	15	2167	6	5	2666	7	15	2839	7	29	
1807	4	7	2395	6	23	2653	7	14	1923	4	16	

*Passes are listed in the same order and position as they appear in Figures 1, 2, 9-11, 18, and 19. Where there is a Part I and a Part II for a particular detector, Part I includes the first, third, etc., line, and Part II, the second, fourth, etc.

TABLE II
(continued)

Disturbed												
Group 1			Group 2			Group 3			Group 4			
Rev. No.	Mo.	Day	Rev. No.	Mo.	Day	Rev. No.	Mo.	Day	Rev. No.	Mo.	Day	
1737	5	1	1881	5	13	2432	6	26	2740	7	21	
1749	5	2	2084	5	29	2855	7	30	2739	7	21	
1773	5	4	2196	6	7	2329	6	18	2764	7	23	
1886	5	13	2081	5	29	2428	6	26	2750	7	21	
2333	6	18	2080	5	29	2441	6	27	1713	4	30	

*Passes are listed in the same order and position as they appear in Figures 1, 2, 9-11, 18, and 19. Where there is a Part I and a Part II for a particular detector, Part I includes the first, third, etc., line, and Part II, the second, fourth, etc.

TABLE III

Ratio of Median Counting Rates:
$R (E_e \geq 40 \text{ keV})/R (E_e \geq 230 \text{ keV})$

Invariant Latitude	Local Time Intervals			
	09:00 to 15:00	15:00 to 21:00	21:00 to 3:00	3:00 to 9:00
45.0	64.8	60.6	138.	63.8
47.5	95.6	100.	115.	101.
50.0	192.	178.	169.	169.
52.5	682.	338.	440.	493.
55.0	754.	360.	491.	582.
57.5	65.2	93.8	60.0	67.3
60.0	8.30	2.10	6.40	9.50
62.5	4.90	4.30	4.20	6.30
65.0	10.2	20.8	21.1	13.3
67.5	52.0	113.	194.	66.7

FIGURE CAPTIONS

Figure 1. Representative quiet day latitude profiles of the directional intensity of electrons $E_e \geq 40$ keV at large pitch angles ($\alpha = 90° \pm 13°$).

Figure 2. Representative disturbed day latitude profiles of the directional intensity of electrons $E_e \geq 40$ keV at large pitch angles ($\alpha = 90° \pm 13°$).

Figure 3. Corrected median latitude profiles of the directional intensity of 40 keV electrons at large pitch angles ($\alpha = 90° \pm 13°$).

Figure 4. Scatter plot of the directional intensity electrons $E_e \geq 40$ keV at large pitch angles ($\alpha = 90° \pm 13°$) versus B for L = 2.2, 2.6.

Figure 5. Continuation of Figure 4 for L = 3.5, 4.5.

Figure 6. Continuation of Figure 4 for L = 6.0, 7.0.

Figure 7. Summary plot of the median directional intensity of electrons $E_e \geq 40$ keV at large pitch angles ($\alpha = 90° \pm 13°$) versus B for all L values in the range $2.0 \leq L \leq 4.0$.

Figure 8. Continuation of Figure 7 for $4.5 \leq L \leq 7.5$.

Figure 9. Representative quiet day latitude profiles of the directional intensity of electrons $E_e \geq 40$ keV at small pitch angles ($\alpha < 43°$). Part I.

Figure 10. Continuation of Figure 9. Part II.

Figure 11. Representative disturbed day latitude profiles of the directional intensity of electrons $E_e \geq 40$ keV at small pitch angles ($\alpha < 43°$).

Figure 12. Corrected median latitude profiles of the directional intensity of 40 keV electrons at small pitch angles ($\alpha < 43°$).

Figure 13. Scatter plot of the directional intensity of 40 keV electrons at small pitch angles ($\alpha < 43°$) versus B for L = 2.2, 2.6.

Figure 14. Continuation of Figure 13 for L = 3.5, 4.5.

Figure 15. Continuation of Figure 13 for L = 5.5, 7.0.

Figure 16. Summary plot of the median directional intensity of 40 keV electrons at small pitch angles ($\alpha < 43°$) versus B for all L values in the range $2.0 \leq L \leq 4.0$.

Figure 17. Continuation of Figure 16 for $4.5 \leq L \leq 7.5$.

Figure 18. Representative quiet day latitude profiles of the directional intensity of electrons $E_e \geq 230$ keV at large pitch angles ($\alpha = 90° \pm 13°$).

Figure 19. Representative disturbed day latitude profiles of the directional intensity of electrons $E_e \geq 230$ keV at large pitch angles ($\alpha = 90° \pm 13°$).

Figure 20. Corrected median latitude profiles of the directional intensity of electrons $E_e \geq 230$ keV at large pitch angles ($\alpha = 90° \pm 13°$).

Figure 21. Scatter plot of the directional intensity of electrons $E_e \geq 230$ keV at large pitch angles ($\alpha = 90° \pm 13°$) versus B for L = 2.2, 2.6.

Figure 22. Continuation of Figure 21 for L = 3.5, 4.5.

Figure 23. Continuation of Figure 21 for L = 6.0, 7.0.

Figure 24. Summary plot of the median directional intensity of electrons $E_e \geq 230$ keV at large pitch angles ($\alpha = 90° \pm 13°$) versus B for all L values in the range $2.0 \leq L \leq 4.0$.

Figure 25. Continuation of Figure 24 for $4.5 \leq L \leq 7.0$.

Figure 26. Scatter plot of the omnidirectional intensity of electrons $E_e \geq 1.6$ MeV versus B for L = 2.0, 2.2.

Figure 27. Continuation of Figure 26 for L = 2.4, 2.6.

Figure 28. Continuation of Figure 26 for L = 2.8, 3.0.

Figure 29. Continuation of Figure 26 for L = 3.5, 4.5.

Figure 30. Continuation of Figure 26 for L = 6.0, 7.0.

Figure 31. Summary plot of the median omnidirectional intensity of electrons $E_e \geq 1.6$ MeV versus B for $4.5 \leq L \leq 6.5$.

Figure 32. Plot of the intersection of omnidirectional intensity versus B curve with B = 0.30 gauss as a function of latitude (λ) for electrons $E_e \geq 1.6$ MeV.

Figure 33. Plot of intensity versus L for revolution 2022 for electrons $E_e \geq 40$ keV, $\alpha = 90° \pm 13°$, $< 43°$; $E_e \geq 230$ keV, $\alpha = 90° \pm 13°$; $E_e \geq 1.6$ MeV, omnidirectional.

Figure 34. Plot of intensity versus L for revolution 1886 for electrons $E_e \geq 40$ keV, $\alpha = 90° \pm 13°$, $< 43°$; $E_e \geq 230$ keV, $\alpha = 90° \pm 13°$; $E_e \geq 1.6$ MeV, omnidirectional.

QUIET DAY LATITUDE PROFILES OF THE DIRECTIONAL INTENSITY OF ELECTRONS $E_e \geq 40$ KeV AT LARGE PITCH ANGLES ($\alpha = 90° \pm 13°$) DURING THE TEN MAGNETICALLY QUIET DAYS PER MONTH IN APRIL, MAY, JUNE AND JULY, 1963

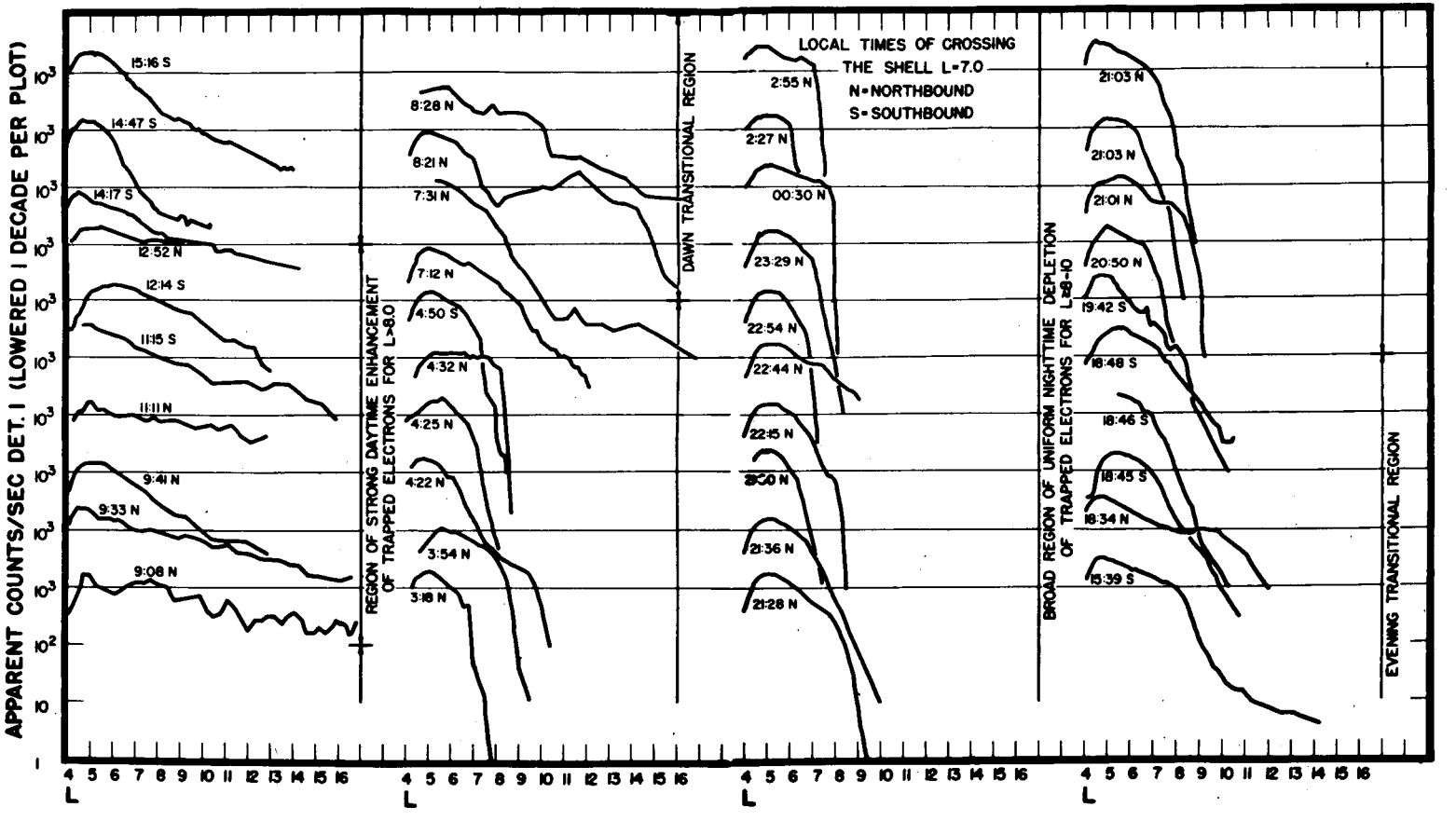

FIGURE 1

DISTURBED DAY LATITUDE PROFILES OF THE DIRECTIONAL INTENSITY OF ELECTRONS $E_e \geq 40$ KeV AT LARGE PITCH ANGLES ($\alpha = 90° \pm 13°$) DURING THE FIVE DISTURBED DAYS PER MONTH IN APRIL, MAY, JUNE AND JULY, 1963

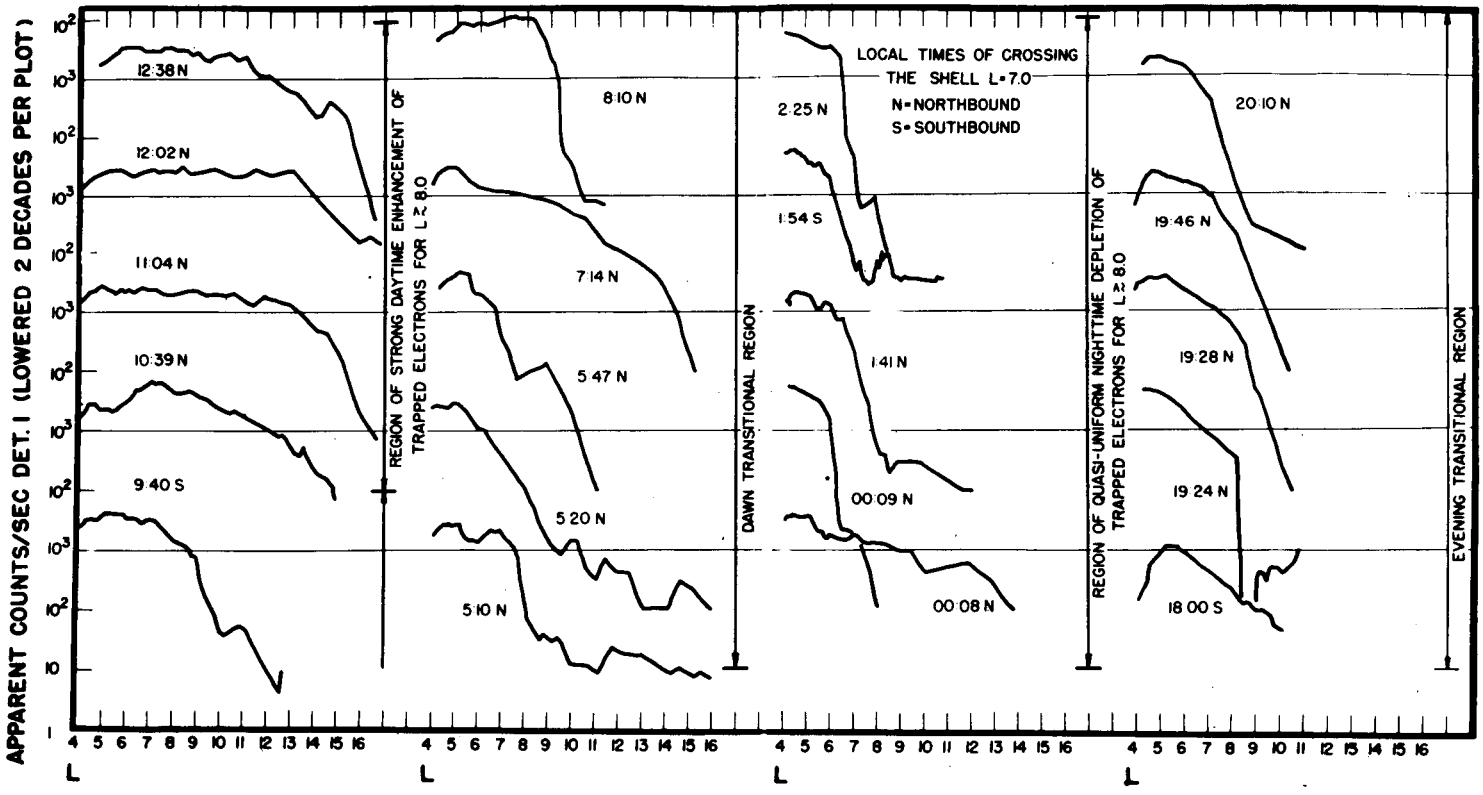

FIGURE 2

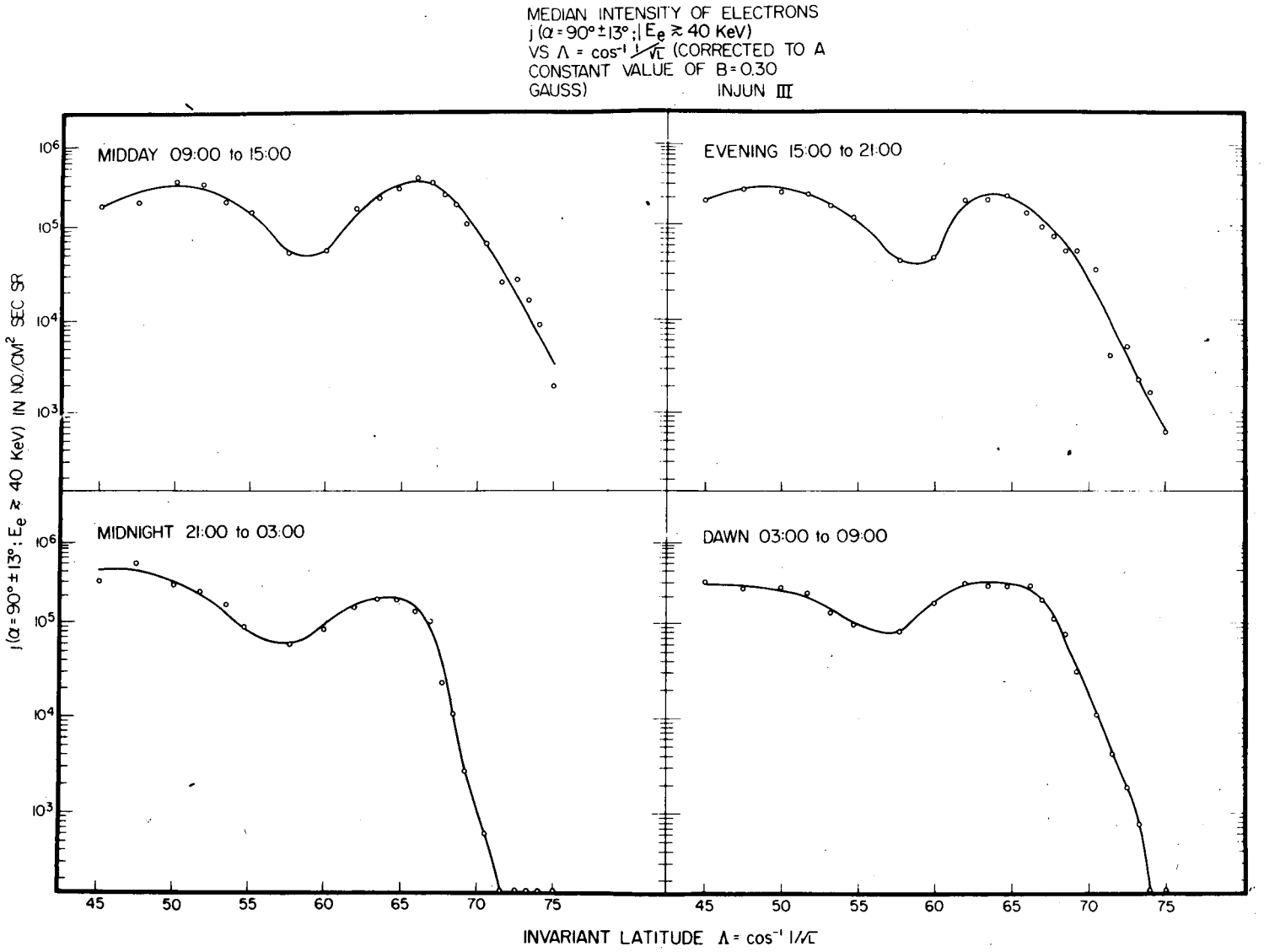
MEDIAN INTENSITY OF ELECTRONS
j (α = 90° ± 13° ; E_e ≳ 40 KeV)
VS Λ = cos⁻¹ 1/√L (CORRECTED TO A
CONSTANT VALUE OF B = 0.30
GAUSS)
INJUN III
MIDDAY 09:00 to 15:00
EVENING 15:00 to 21:00
MIDNIGHT 21:00 to 03:00
DAWN 03:00 to 09:00
j (α = 90° ± 13° ; E_e ≳ 40 KeV) IN NO./CM² SEC SR
10⁶
10⁵
10⁴
10³
45
50
55
60
65
70
75
INVARIANT LATITUDE Λ = cos⁻¹ 1/√L

FIGURE 3

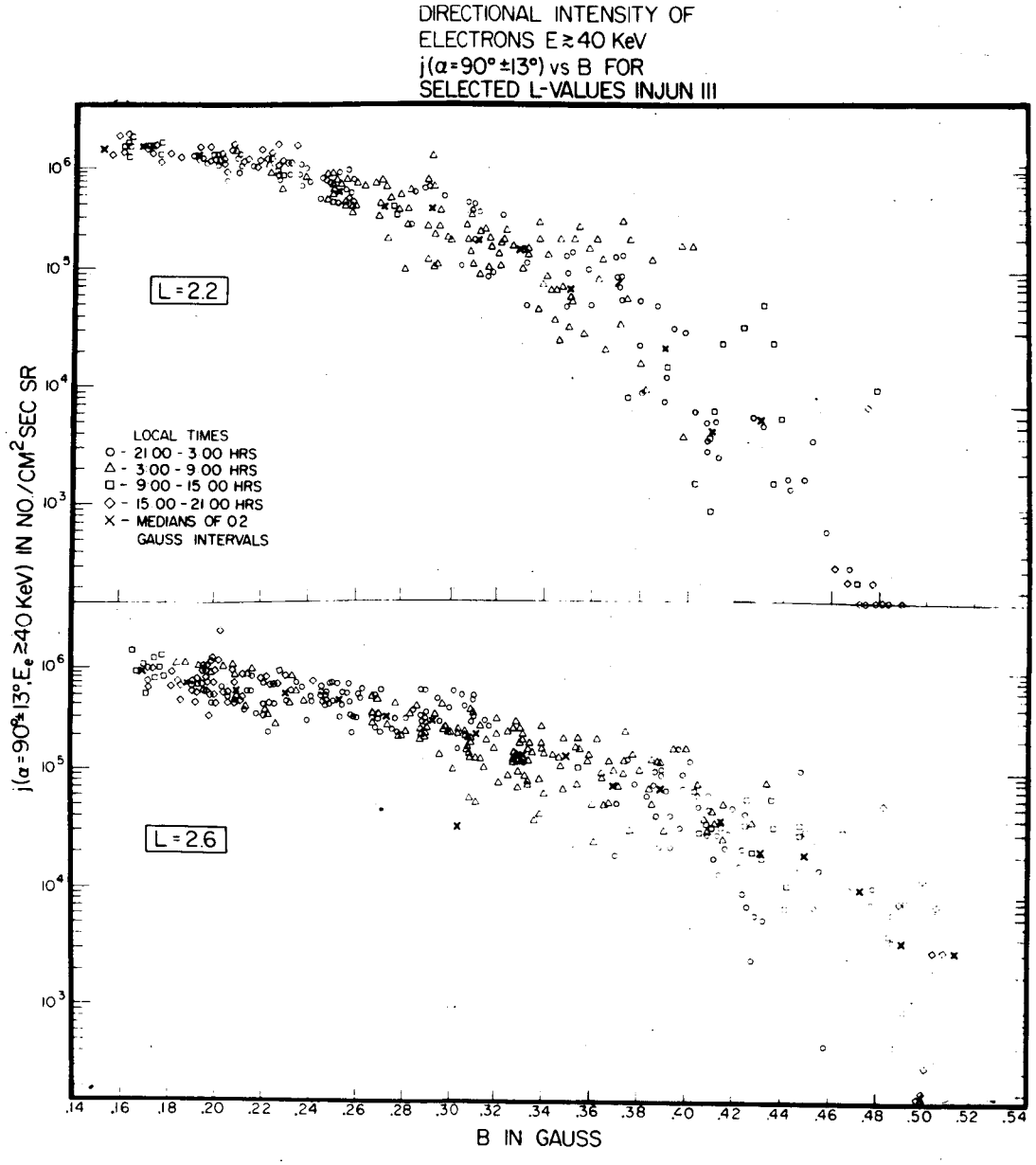
DIRECTIONAL INTENSITY OF
ELECTRONS E≳40 KeV
j(α=90°±13°) vs B FOR
SELECTED L-VALUES INJUN III
L=2.2
L=2.6
LOCAL TIMES
○ - 21 00 - 3 00 HRS
△ - 3 00 - 9 00 HRS
□ - 9 00 - 15 00 HRS
◇ - 15 00 - 21 00 HRS
× - MEDIANS OF 02
GAUSS INTERVALS
j(α=90°±13°,E_e ≥40 KeV) IN NO./CM²SEC SR
B IN GAUSS

FIGURE 4

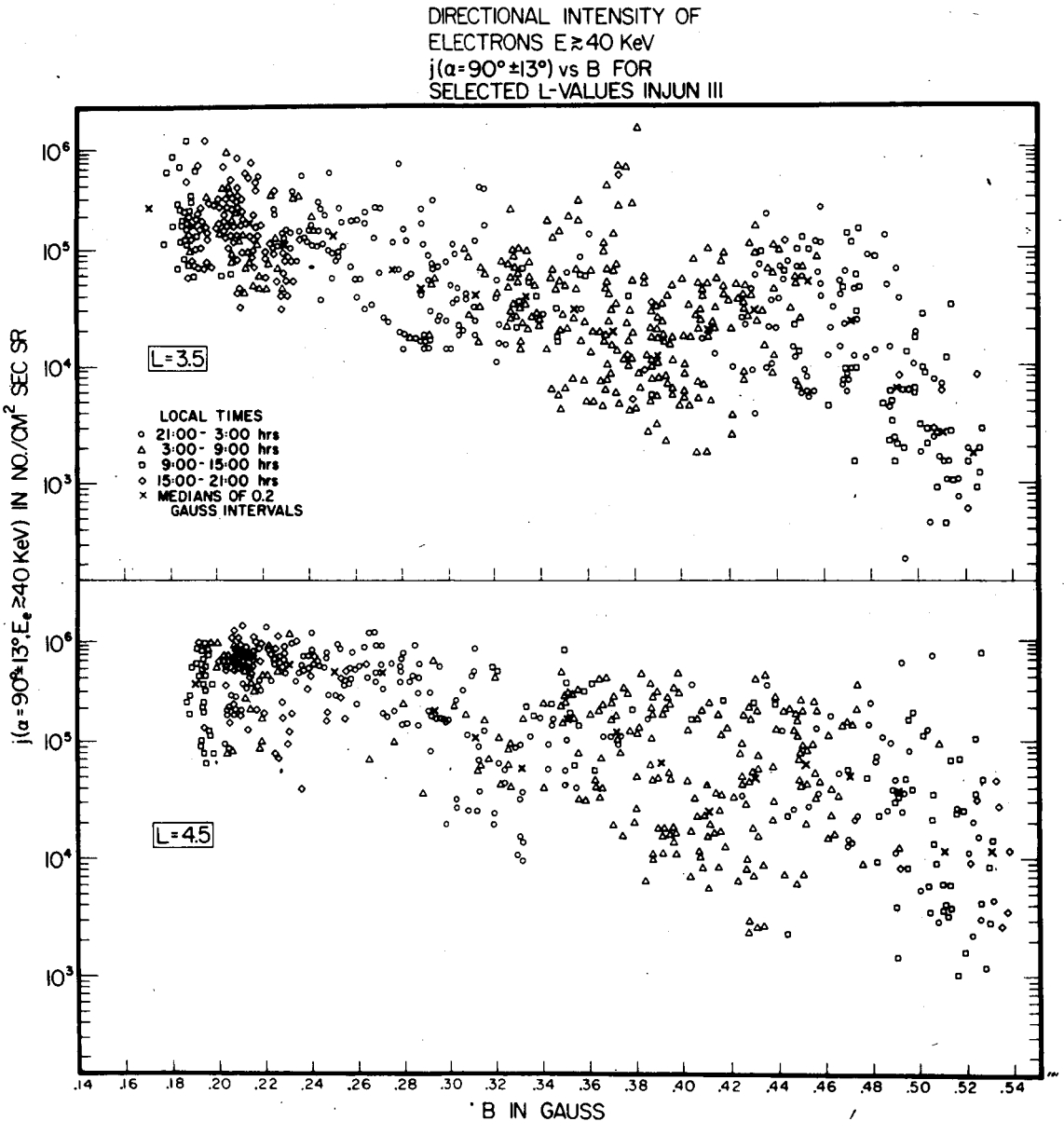
DIRECTIONAL INTENSITY OF
ELECTRONS E≳40 KeV
j(α=90°±13°) vs B FOR
SELECTED L-VALUES INJUN III
j(α=90°±13°,E_e≥40 KeV) IN NO./CM² SEC SR
L=3.5
LOCAL TIMES
21:00- 3:00 hrs
3:00- 9:00 hrs
9:00-15:00 hrs
15:00-21:00 hrs
MEDIANS OF 0.2 GAUSS INTERVALS
L=4.5
B IN GAUSS

FIGURE 5

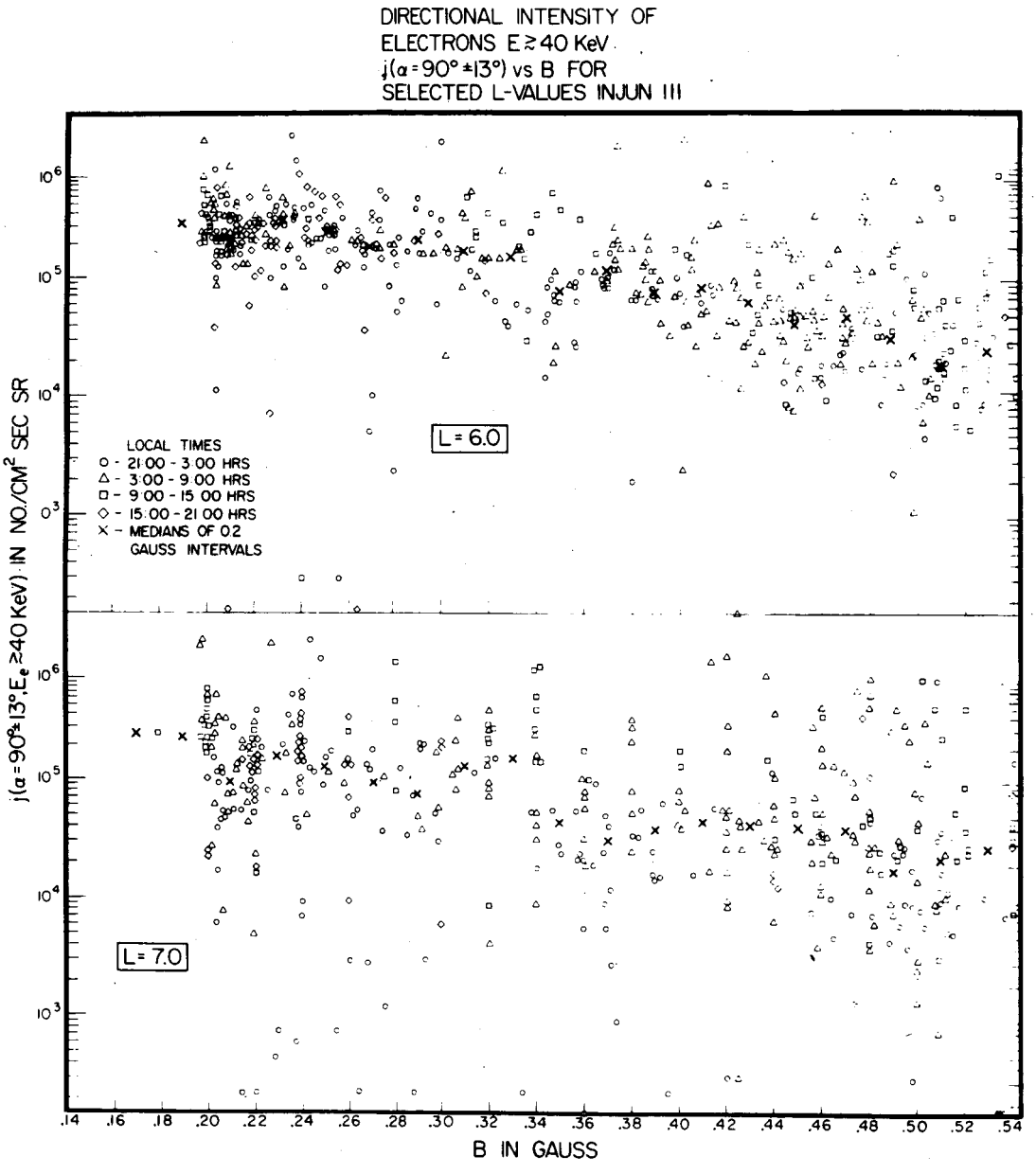
DIRECTIONAL INTENSITY OF
ELECTRONS E≥40 KeV
j(α=90°±13°) vs B FOR
SELECTED L-VALUES INJUN III
LOCAL TIMES
○ - 21:00 - 3:00 HRS
△ - 3:00 - 9:00 HRS
□ - 9:00 - 15:00 HRS
◇ - 15:00 - 21:00 HRS
× - MEDIANS OF 0.2
GAUSS INTERVALS
L=6.0
L=7.0
j(α=90°±13°,E_e≥40 KeV) IN NO./CM² SEC SR
B IN GAUSS

FIGURE 6

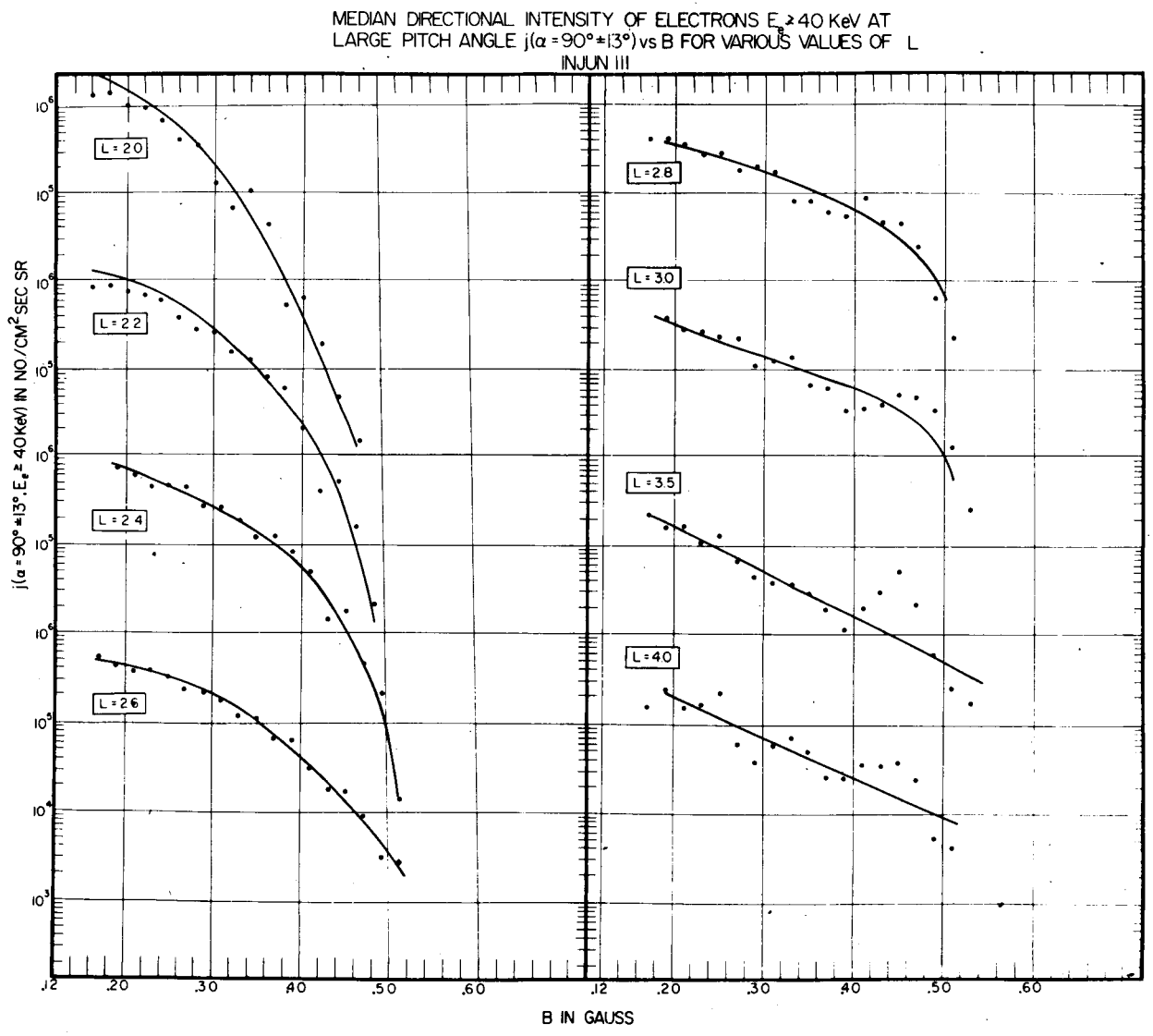
MEDIAN DIRECTIONAL INTENSITY OF ELECTRONS E ≥ 40 KeV AT
LARGE PITCH ANGLE j(α = 90° ± 13°) vs B FOR VARIOUS VALUES OF L
INJUN III
L = 2.0
L = 2.2
L = 2.4
L = 2.6
L = 2.8
L = 3.0
L = 3.5
L = 4.0
j(α = 90° ± 13°, E_e ≥ 40 KeV) IN NO./CM² SEC SR
B IN GAUSS
.12
.20
.30
.40
.50
.60

FIGURE 7

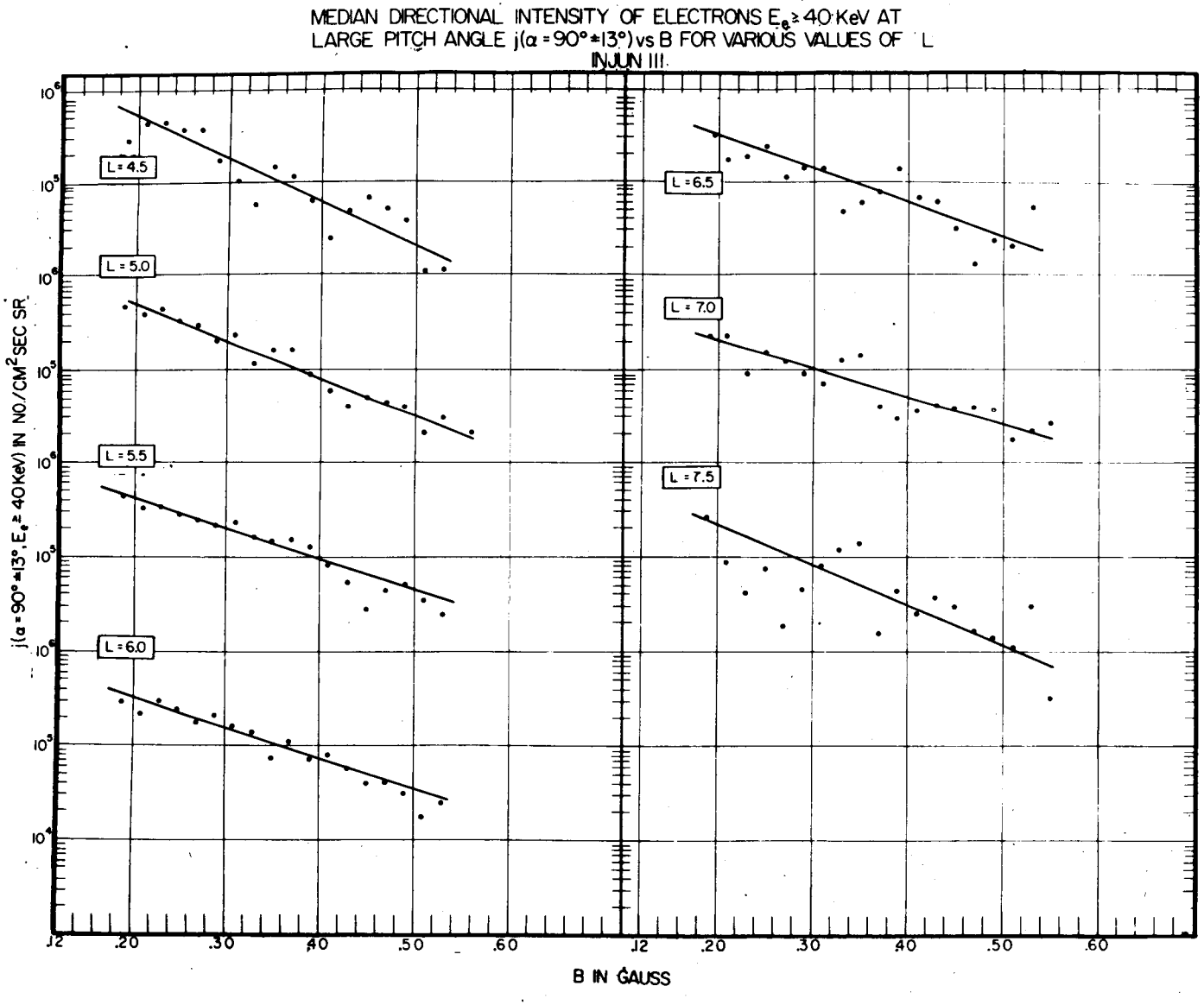
MEDIAN DIRECTIONAL INTENSITY OF ELECTRONS $E_e \geq 40$ KeV AT LARGE PITCH ANGLE $j(\alpha = 90° \pm 13°)$ vs B FOR VARIOUS VALUES OF L
INJUN III
L = 4.5
L = 5.0
L = 5.5
L = 6.0
L = 6.5
L = 7.0
L = 7.5
$j(\alpha = 90° \pm 13°, E_e \geq 40 KeV)$ IN NO./CM^{2}SEC SR
B IN GAUSS
.12
.20
.30
.40
.50
.60

FIGURE 8

QUIET DAY LATITUDE PROFILES OF THE DIRECTIONAL INTENSITY OF ELECTRONS $E_e \geq 40$ KeV AT SMALL PITCH ANGLES ($\alpha = 0° \pm 43°$) DURING THE TEN QUIET DAYS PER MONTH IN APRIL, MAY, JUNE AND JULY, 1963 PART I

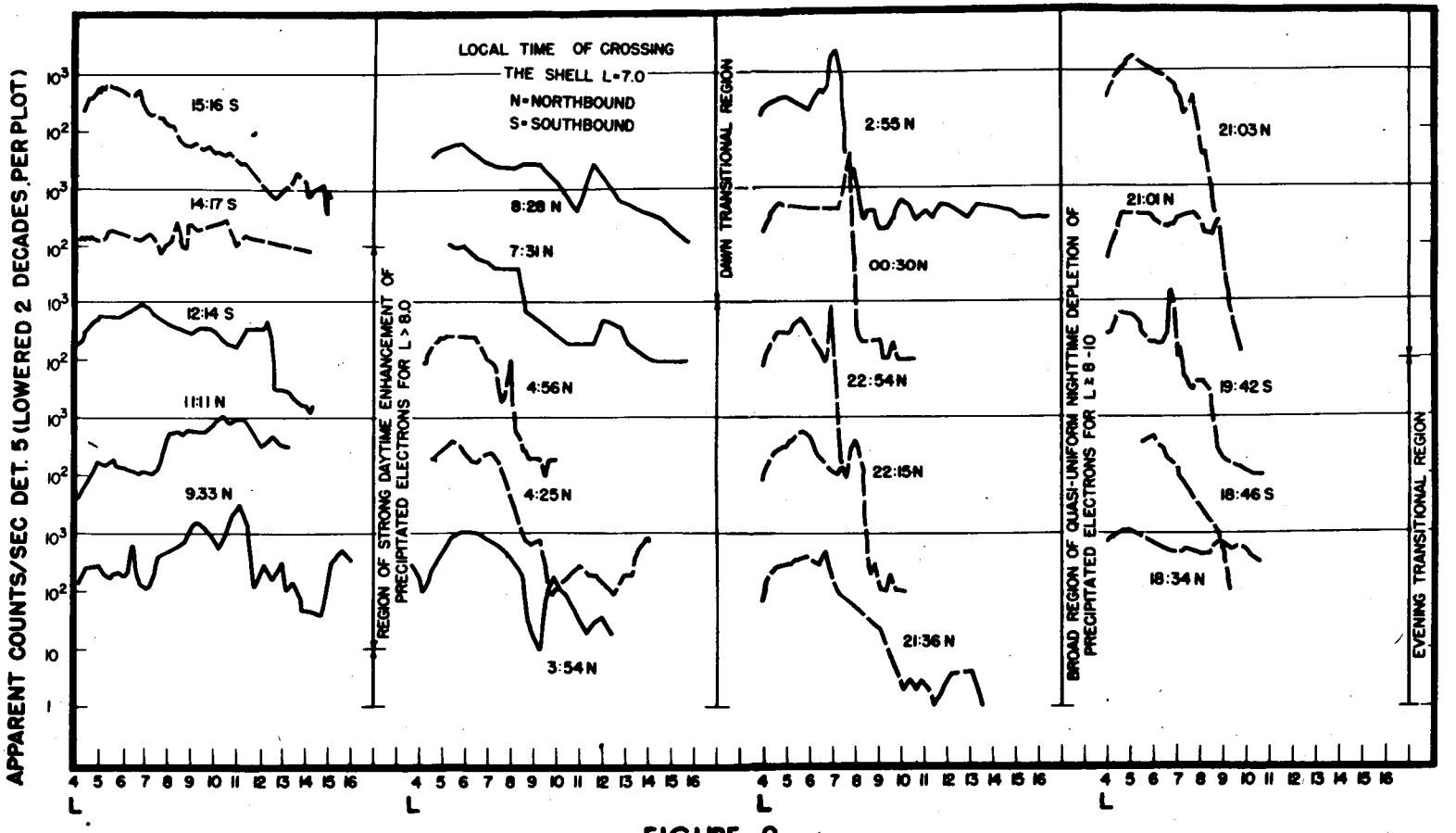

FIGURE 9

QUIET DAY LATITUDE PROFILES OF THE DIRECTIONAL INTENSITY OF ELECTRONS $E_e \geq 40$ KeV AT SMALL PITCH ANGLES ($\alpha = 0° \pm 43°$) DURING THE TEN MAGNETICALLY QUIET DAYS PER MONTH IN APRIL, MAY, JUNE AND JULY, 1963 PART II

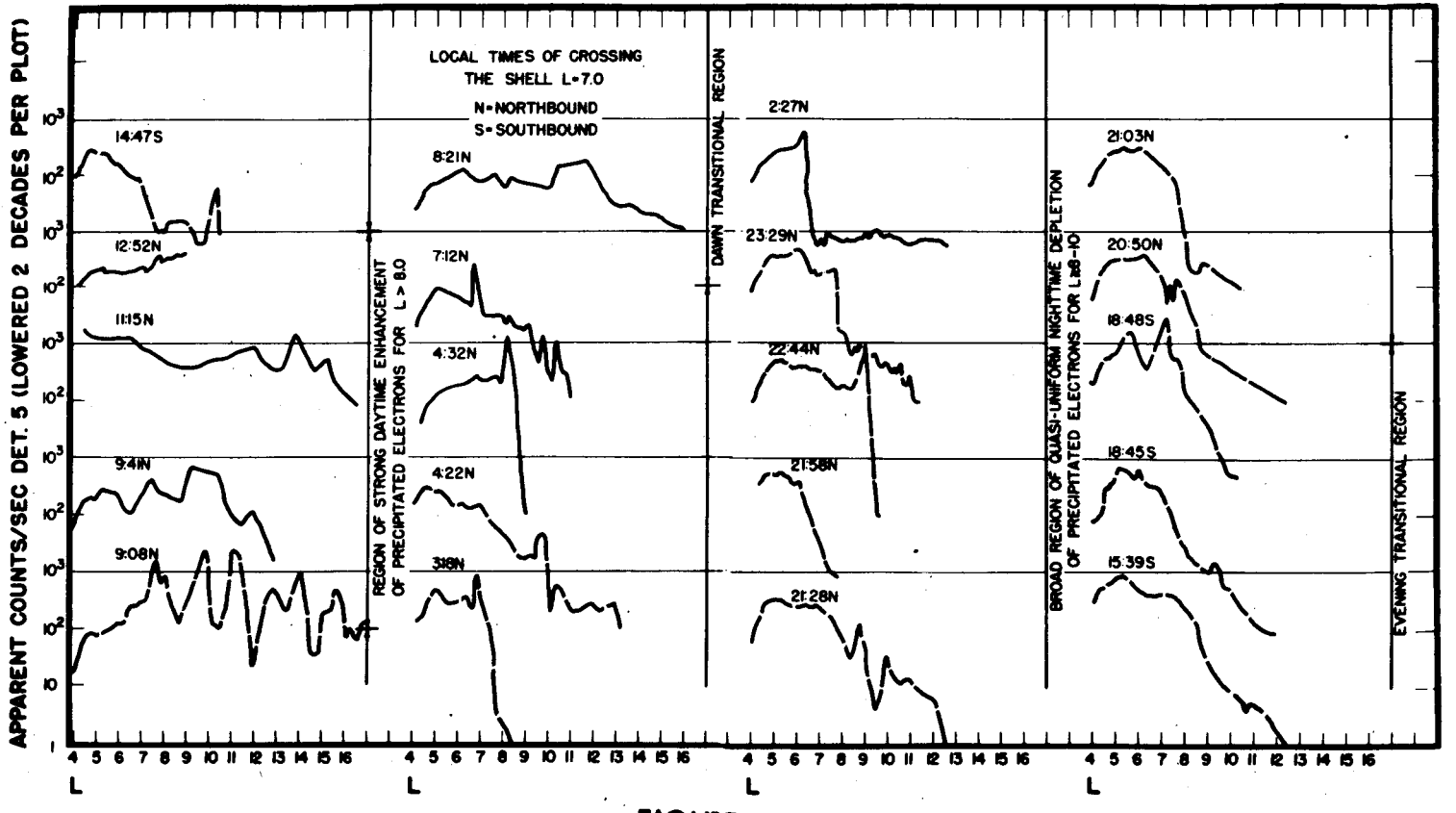

FIGURE 10

DISTURBED DAY LATITUDE PROFILES OF THE DIRECTIONAL INTENSITY OF ELECTRONS $E_e \geq 40$ KeV AT SMALL PITCH ANGLES ($\alpha = 0° \pm 43°$) DURING THE FIVE MAGNETICALLY DISTURBED DAYS PER MONTH IN APRIL, MAY, JUNE AND JULY, 1963

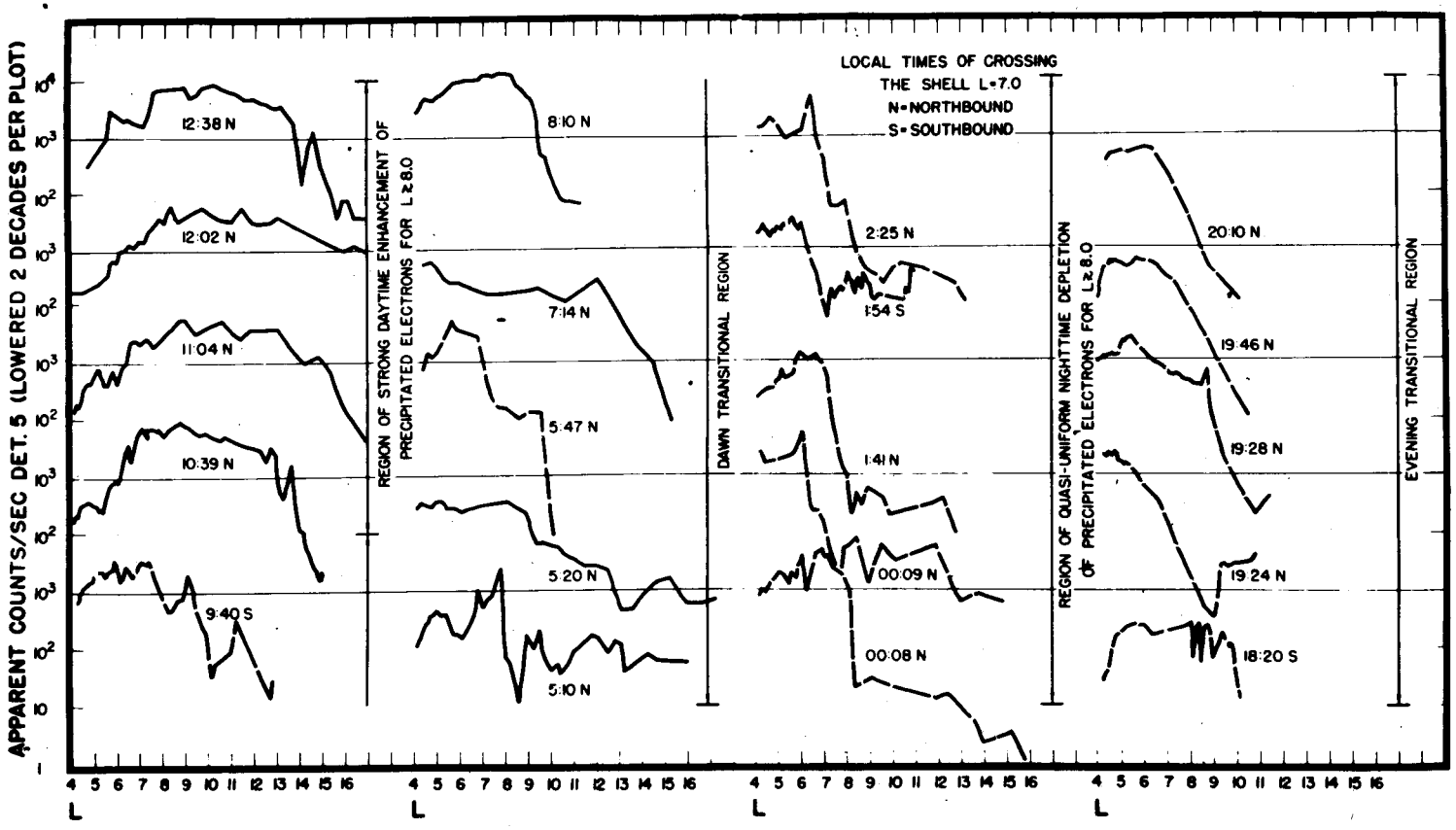

FIGURE 11

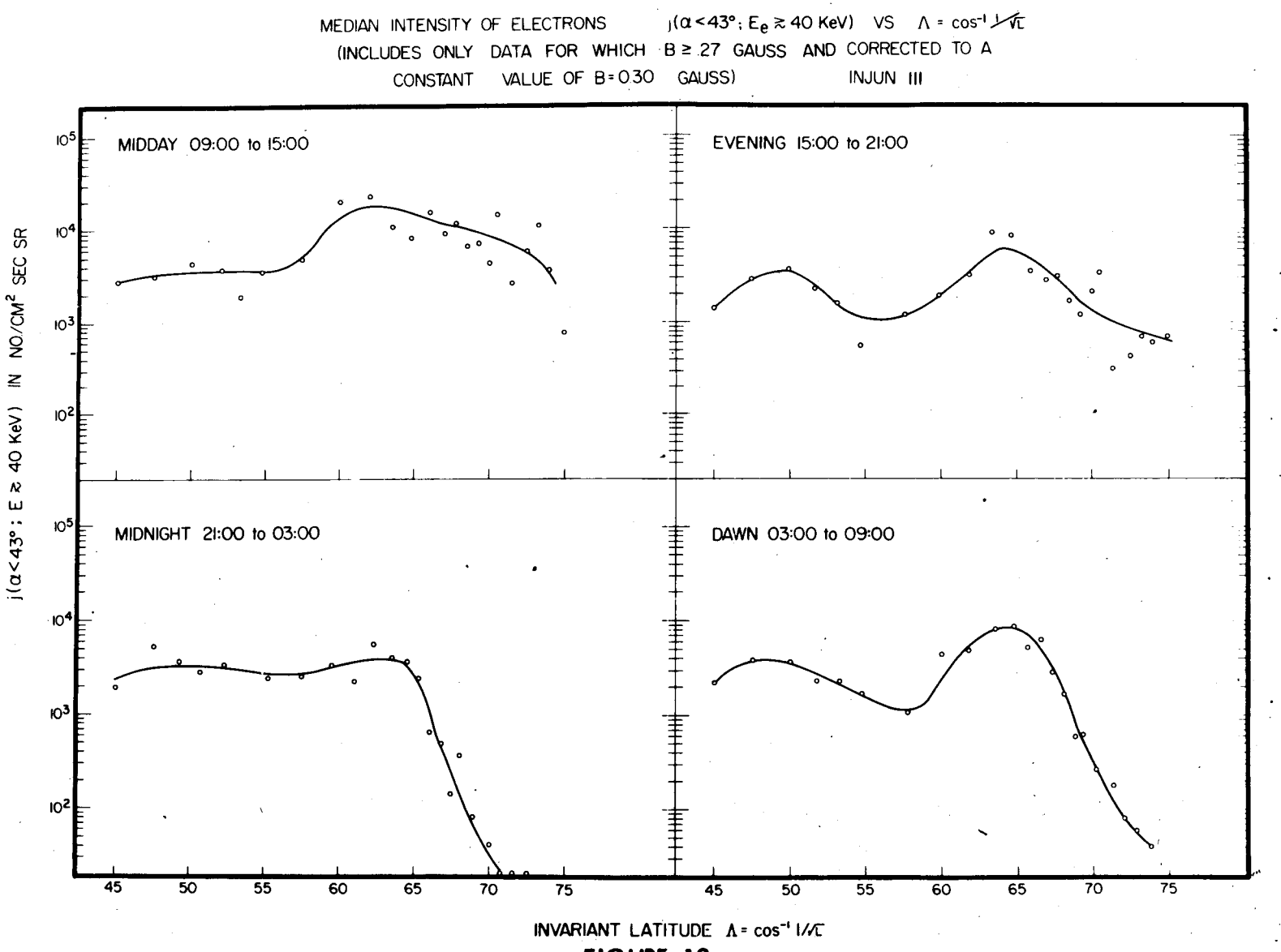
MEDIAN INTENSITY OF ELECTRONS j(α<43°; Ee ≥ 40 KeV) VS Λ = cos⁻¹ 1/√L
(INCLUDES ONLY DATA FOR WHICH B ≥ 27 GAUSS AND CORRECTED TO A
CONSTANT VALUE OF B=0.30 GAUSS) INJUN III
MIDDAY 09:00 to 15:00
EVENING 15:00 to 21:00
MIDNIGHT 21:00 to 03:00
DAWN 03:00 to 09:00
j(α<43°; E ≥ 40 KeV) IN NO/CM² SEC SR
INVARIANT LATITUDE Λ = cos⁻¹ 1/√L

FIGURE 12

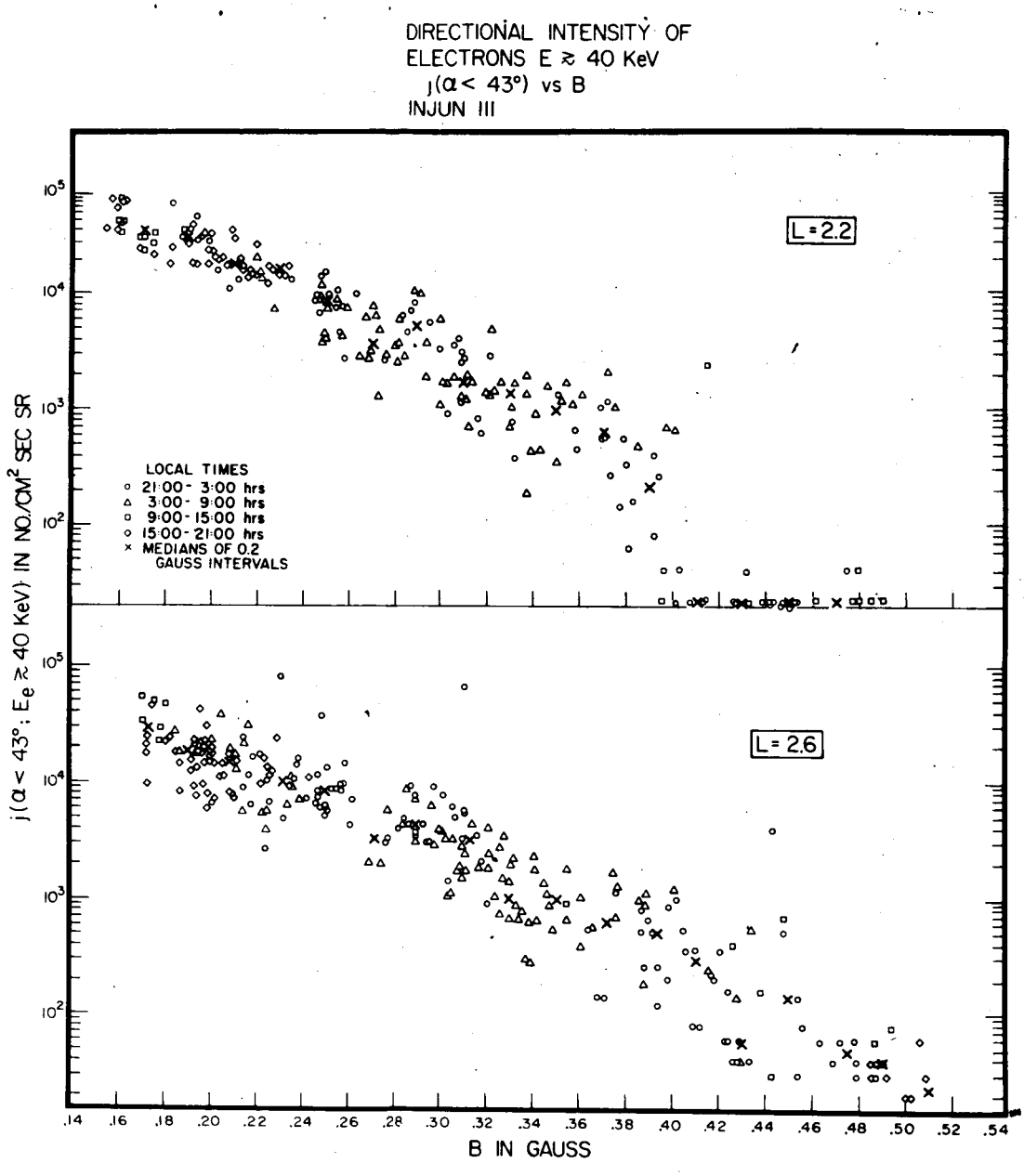
DIRECTIONAL INTENSITY OF
ELECTRONS E ≳ 40 KeV
j(α < 43°) vs B
INJUN III
L = 2.2
L = 2.6
LOCAL TIMES
21:00 - 3:00 hrs
3:00 - 9:00 hrs
9:00 - 15:00 hrs
15:00 - 21:00 hrs
MEDIANS OF 0.2 GAUSS INTERVALS
j(α < 43°; Ee ≳ 40 KeV) IN NO./CM² SEC SR
B IN GAUSS
.14 .16 .18 .20 .22 .24 .26 .28 .30 .32 .34 .36 .38 .40 .42 .44 .46 .48 .50 .52 .54

FIGURE 13

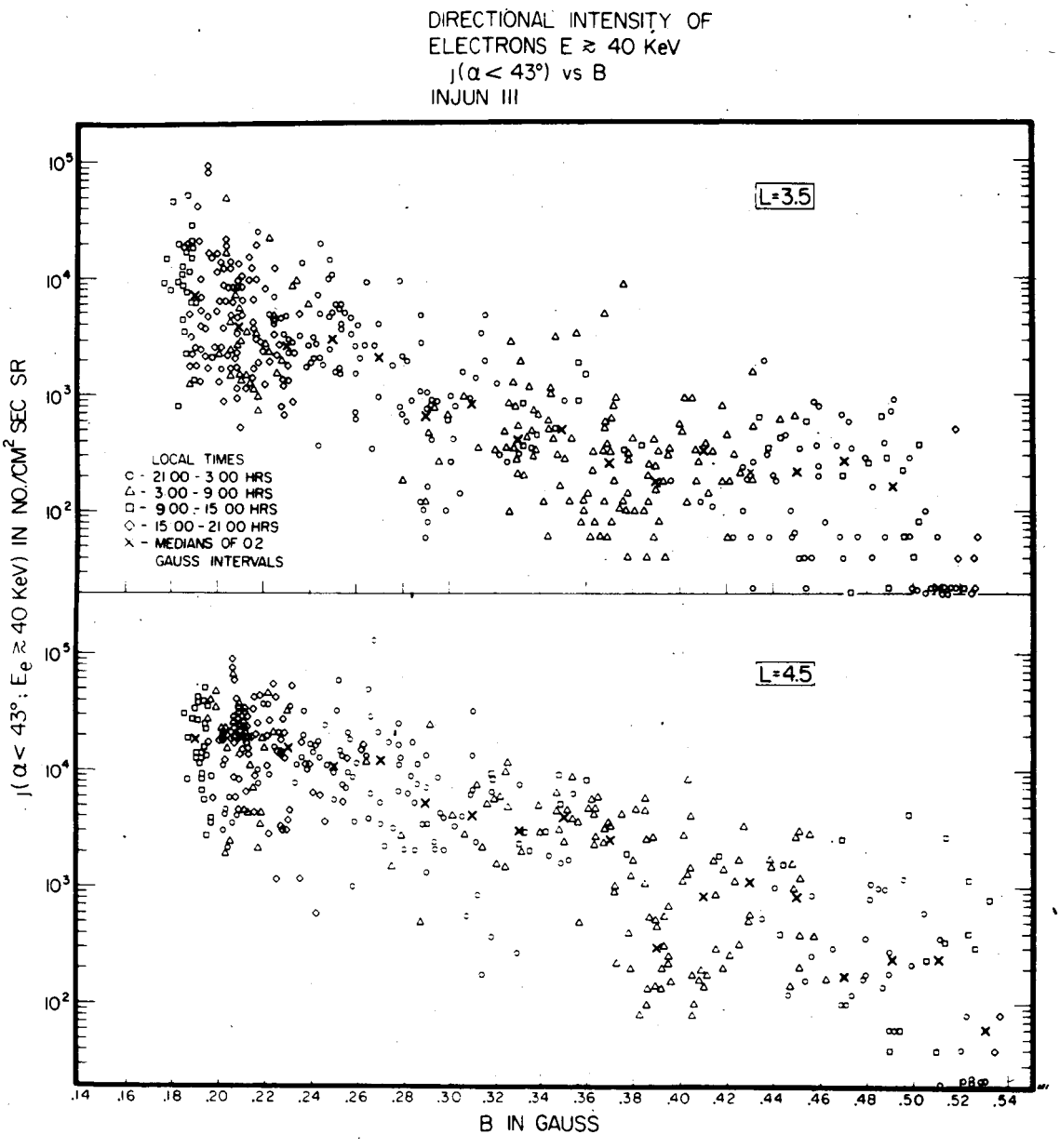
DIRECTIONAL INTENSITY OF
ELECTRONS E ≥ 40 KeV
j(α < 43°) vs B
INJUN III
L=3.5
L=4.5
LOCAL TIMES
○ - 21 00 - 3 00 HRS
△ - 3 00 - 9 00 HRS
□ - 9 00 - 15 00 HRS
◇ - 15 00 - 21 00 HRS
× - MEDIANS OF 02 GAUSS INTERVALS
j(α < 43°; Eₑ ≥ 40 KeV) IN NO./CM² SEC SR
B IN GAUSS

FIGURE 14

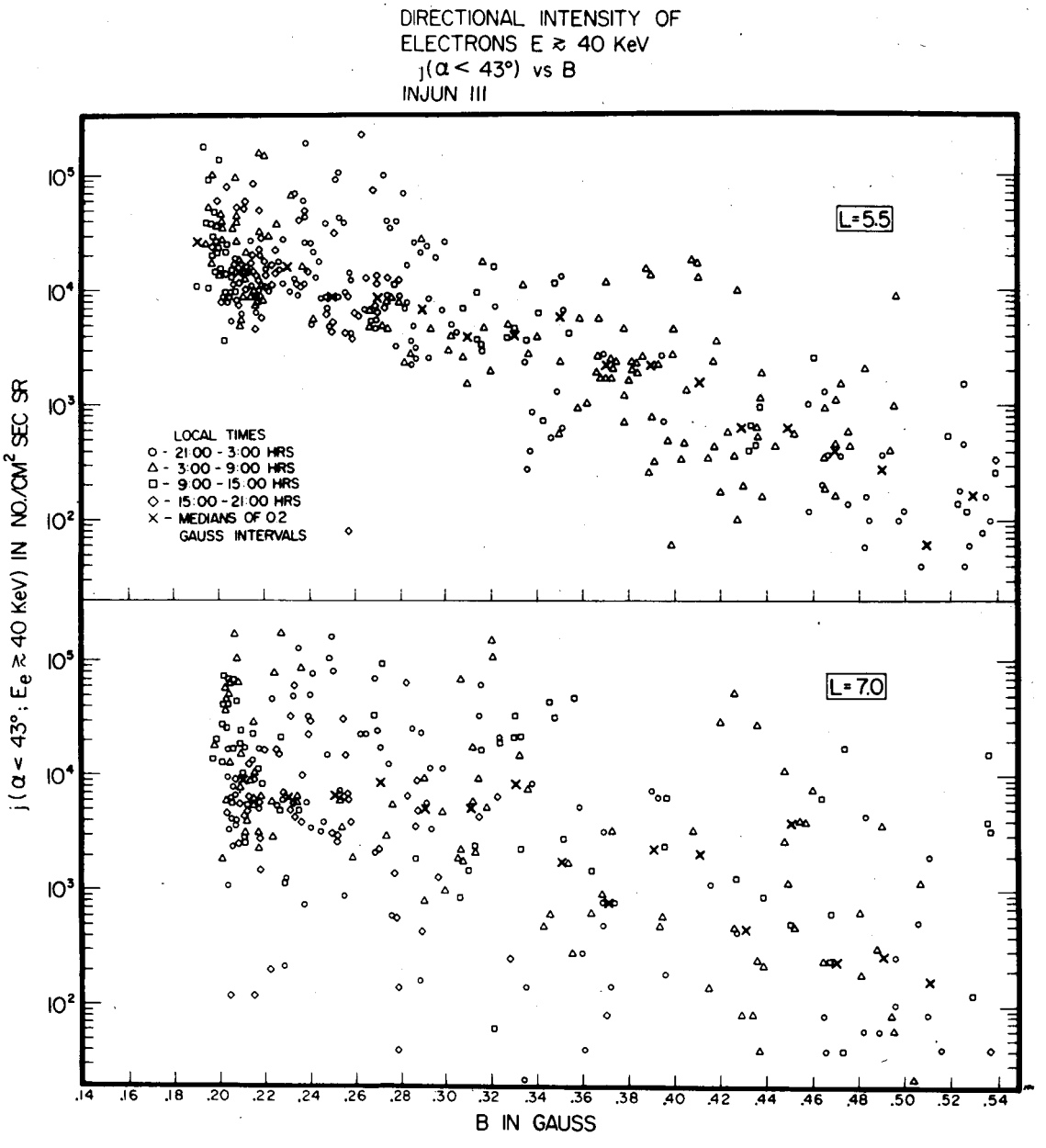
DIRECTIONAL INTENSITY OF
ELECTRONS E ≳ 40 KeV
j(α < 43°) vs B
INJUN III
L=5.5
L=7.0
LOCAL TIMES
○ - 21:00 - 3:00 HRS
△ - 3:00 - 9:00 HRS
□ - 9:00 - 15:00 HRS
◇ - 15:00 - 21:00 HRS
× - MEDIANS OF 02 GAUSS INTERVALS
j(α < 43°; Ee ≳ 40 KeV) IN NO./CM² SEC SR
B IN GAUSS

FIGURE 15

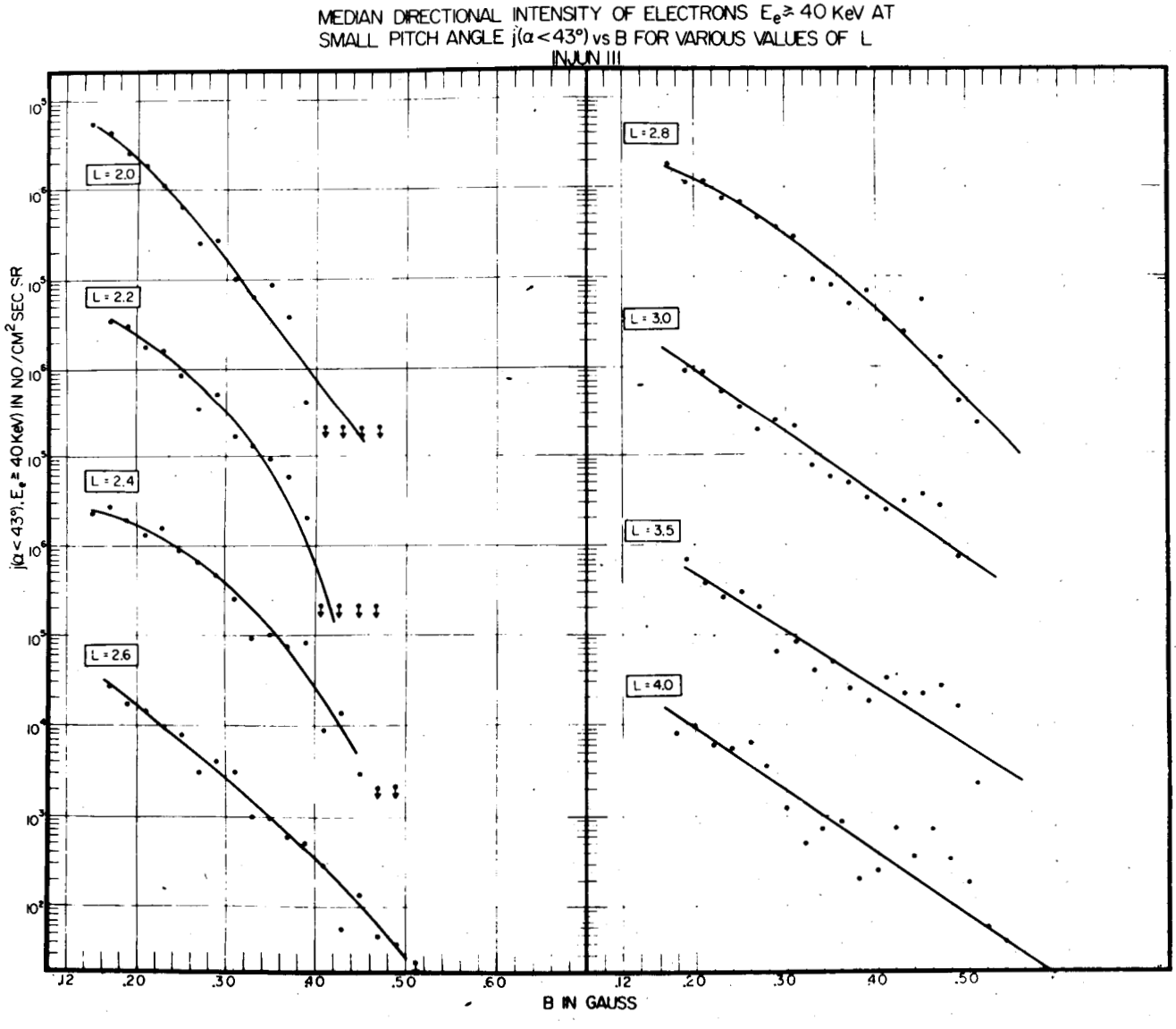
MEDIAN DIRECTIONAL INTENSITY OF ELECTRONS $E_e \geq 40$ KeV AT SMALL PITCH ANGLE $j(\alpha < 43°)$ vs B FOR VARIOUS VALUES OF L
IN JUN III
L = 2.0
L = 2.2
L = 2.4
L = 2.6
L = 2.8
L = 3.0
L = 3.5
L = 4.0
$j(\alpha < 43°), E_e \geq 40$KeV) IN NO./CM^2 SEC SR
B IN GAUSS
.12
.20
.30
.40
.50
.60

FIGURE 16

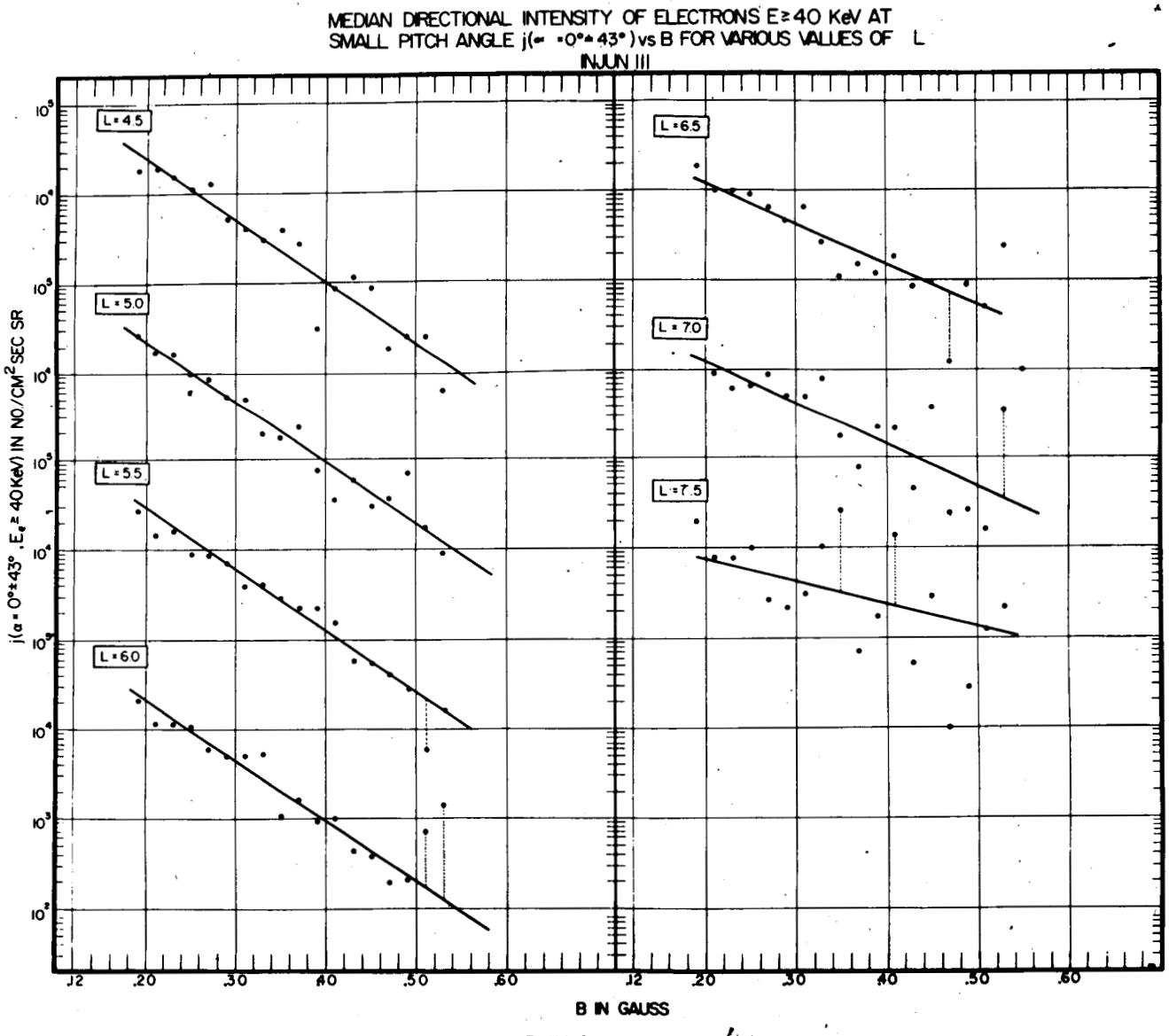
MEDIAN DIRECTIONAL INTENSITY OF ELECTRONS E ≥ 40 KeV AT SMALL PITCH ANGLE j(= 0°±43°) vs B FOR VARIOUS VALUES OF L
INJUN III
L=4.5
L=5.0
L=5.5
L=6.0
L=6.5
L=7.0
L=7.5
j(α = 0°±43°, E_e ≥ 40 KeV) IN NO./CM² SEC SR
B IN GAUSS

FIGURE 17

QUIET DAY LATITUDE PROFILES OF THE DIRECTIONAL INTENSITY OF ELECTRONS $E_e \geq 230$ KeV AT LARGE PITCH ANGLES ($\alpha = 90° \pm 13°$) DURING THE TEN MAGNETICALLY QUIET DAYS PER MONTH IN APRIL, MAY, JUNE AND JULY, 1963

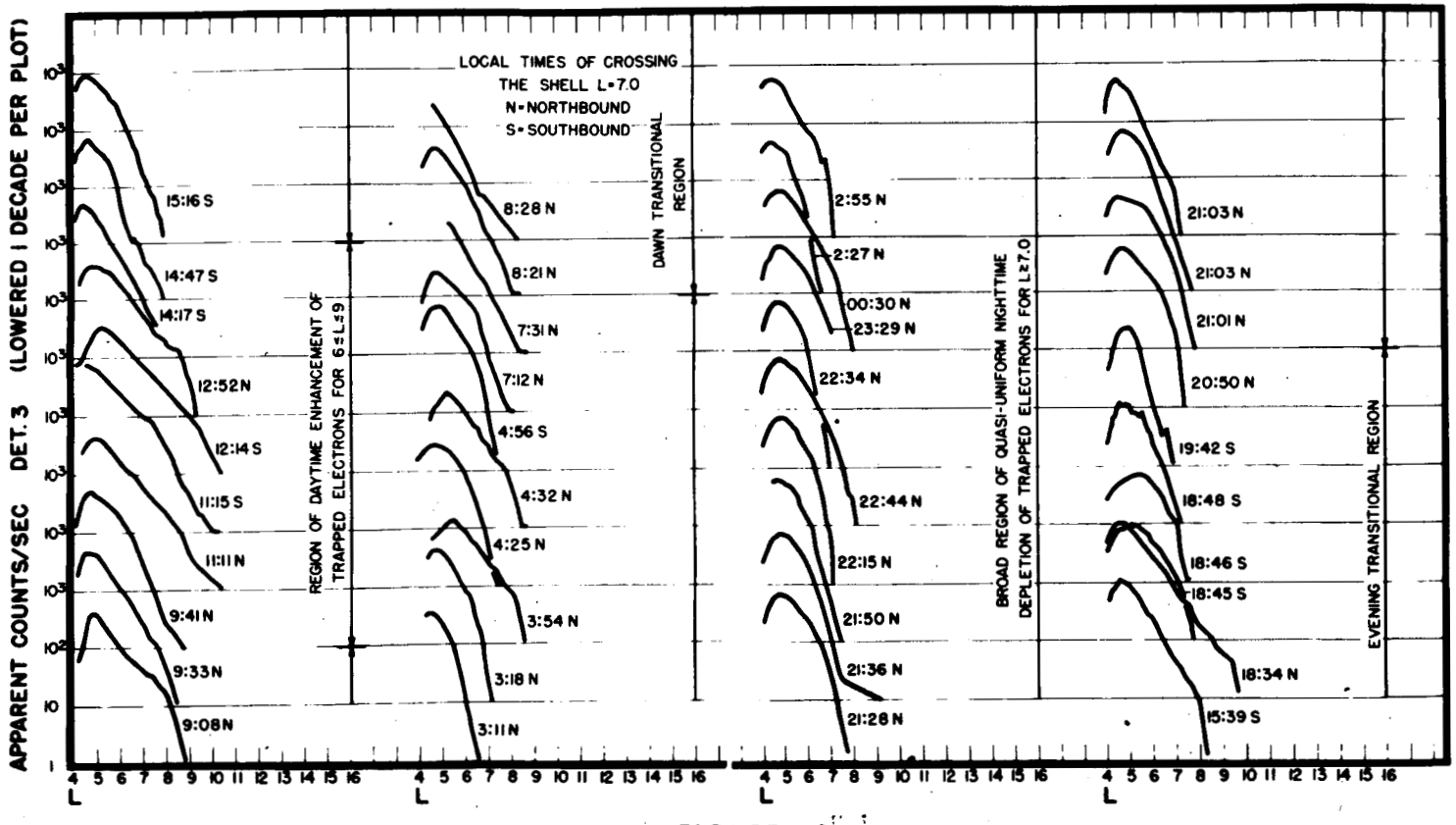

FIGURE 18

DISTURBED DAY LATITUDE PROFILES OF THE DIRECTIONAL INTENSITY OF ELECTRONS $E_e \geq 230$ KeV AT LARGE PITCH ANGLES ($\alpha = 90° \pm 13°$) DURING THE FIVE MAGNETICALLY DISTURBED DAYS PER MONTH IN APRIL, MAY, JUNE AND JULY, 1963

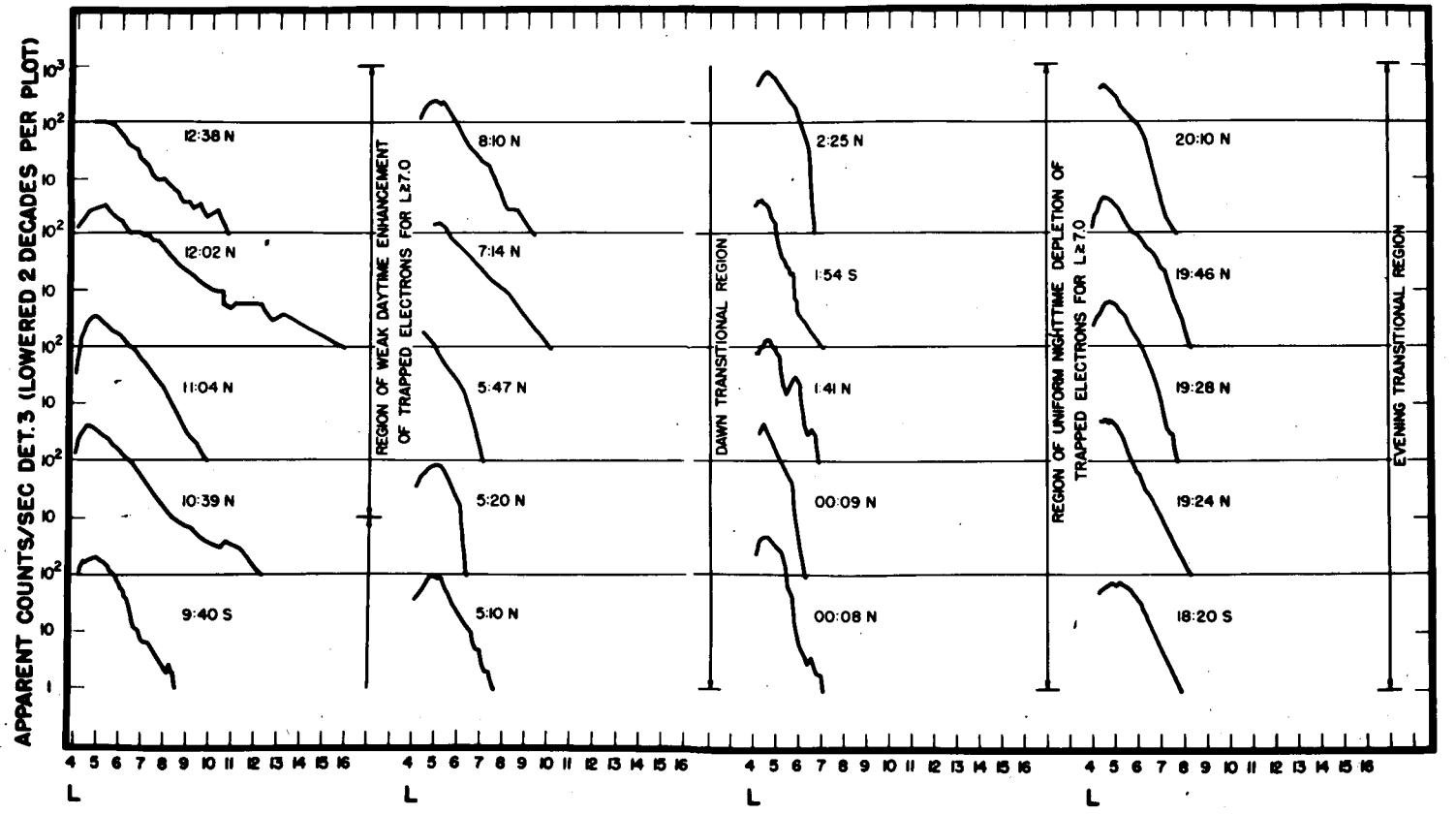

FIGURE 19

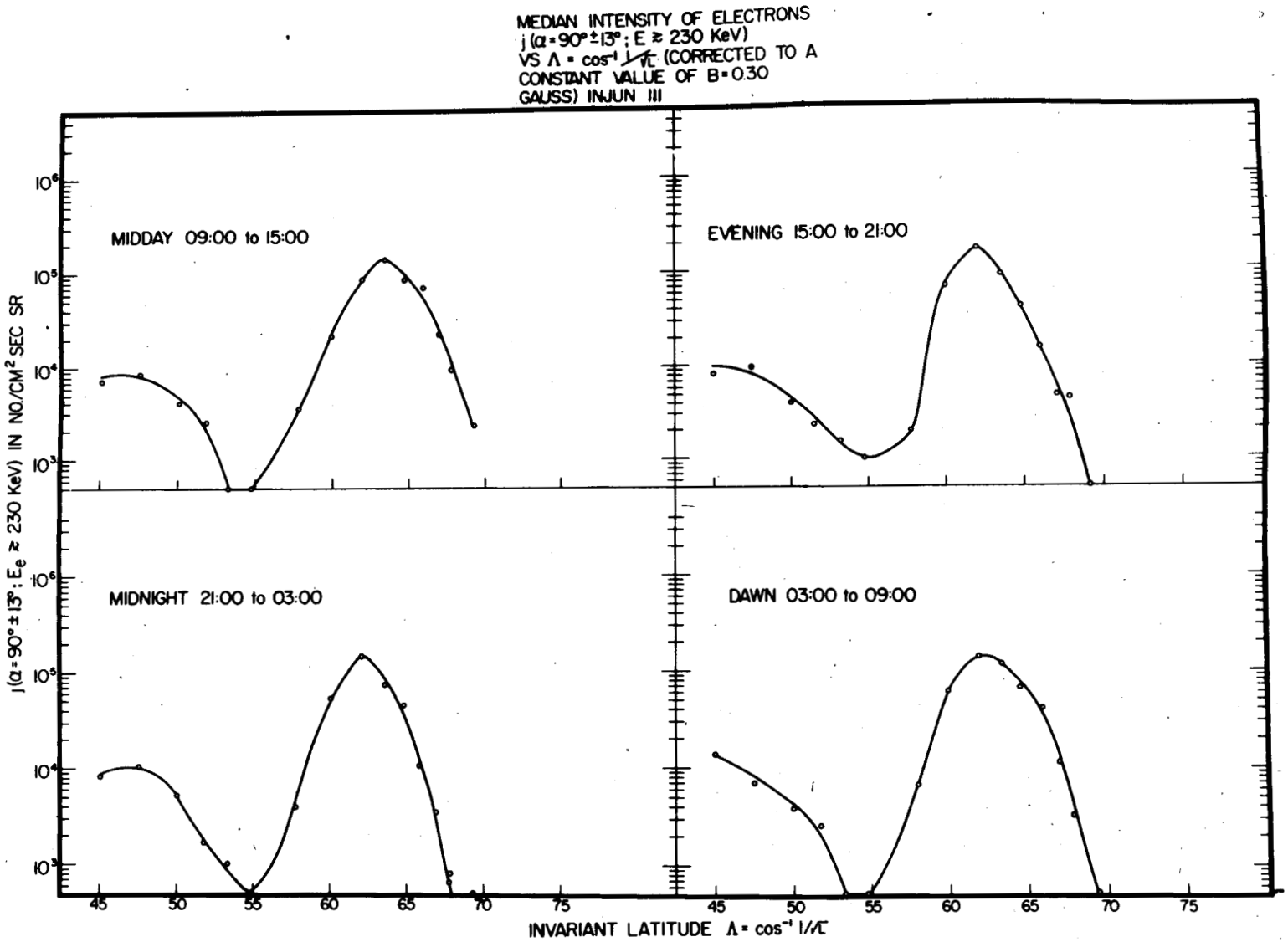
MEDIAN INTENSITY OF ELECTRONS
j (α = 90° ± 13° ; E ≥ 230 KeV)
VS Λ = cos⁻¹ 1/√L (CORRECTED TO A
CONSTANT VALUE OF B = 0.30
GAUSS) INJUN III
MIDDAY 09:00 to 15:00
EVENING 15:00 to 21:00
MIDNIGHT 21:00 to 03:00
DAWN 03:00 to 09:00
j(α = 90° ± 13° ; Ee ≥ 230 KeV) IN NO./CM² SEC SR
INVARIANT LATITUDE Λ = cos⁻¹ 1/√L

FIGURE 20

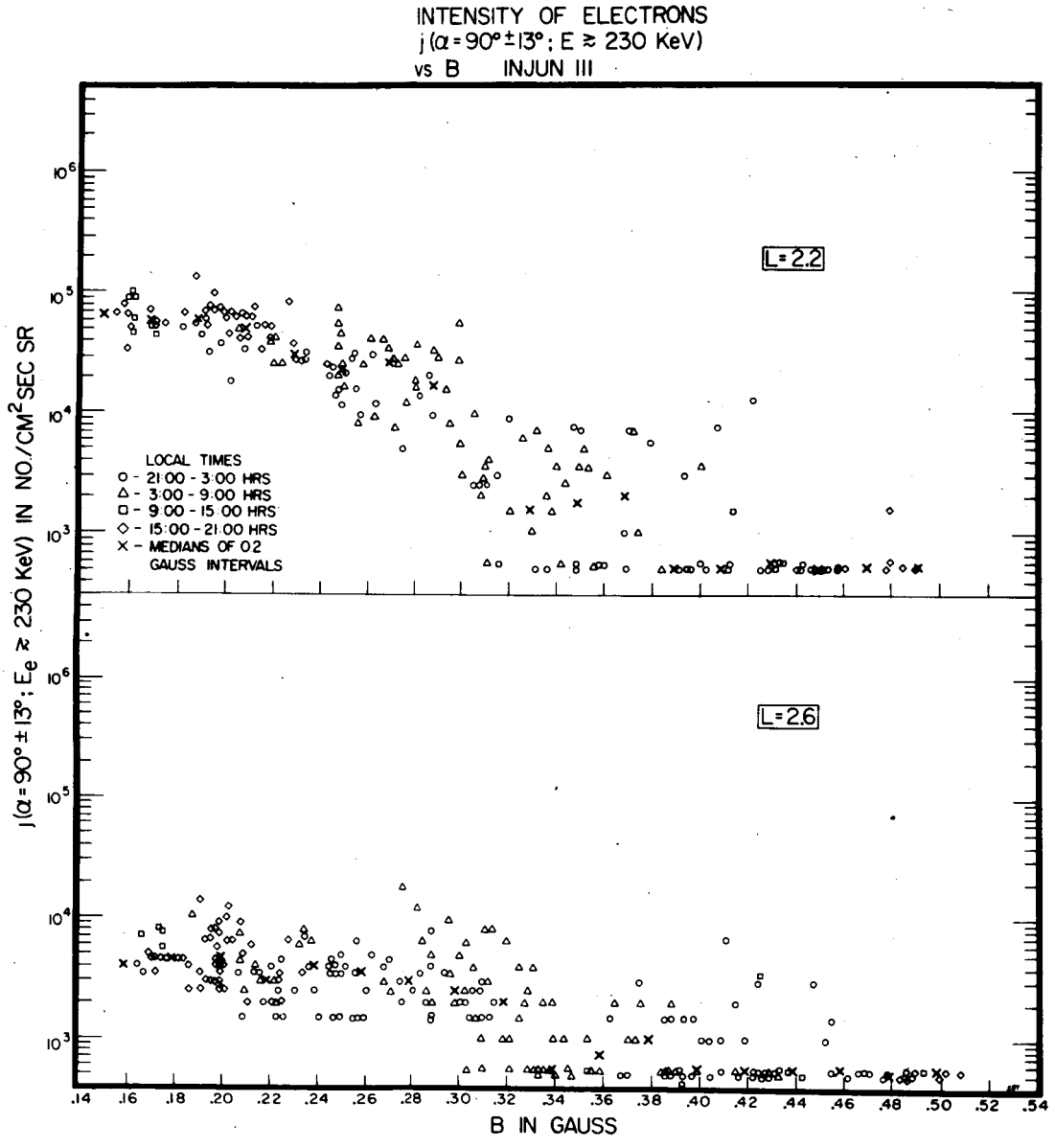
INTENSITY OF ELECTRONS
j(α = 90° ± 13°; E ≥ 230 KeV)
vs B INJUN III
L=2.2
L=2.6
LOCAL TIMES
○ - 21:00 - 3:00 HRS
△ - 3:00 - 9:00 HRS
□ - 9:00 - 15:00 HRS
◇ - 15:00 - 21:00 HRS
× - MEDIANS OF 02 GAUSS INTERVALS
j(α = 90° ± 13°; Ee ≥ 230 KeV) IN NO./CM² SEC SR
B IN GAUSS

FIGURE 21

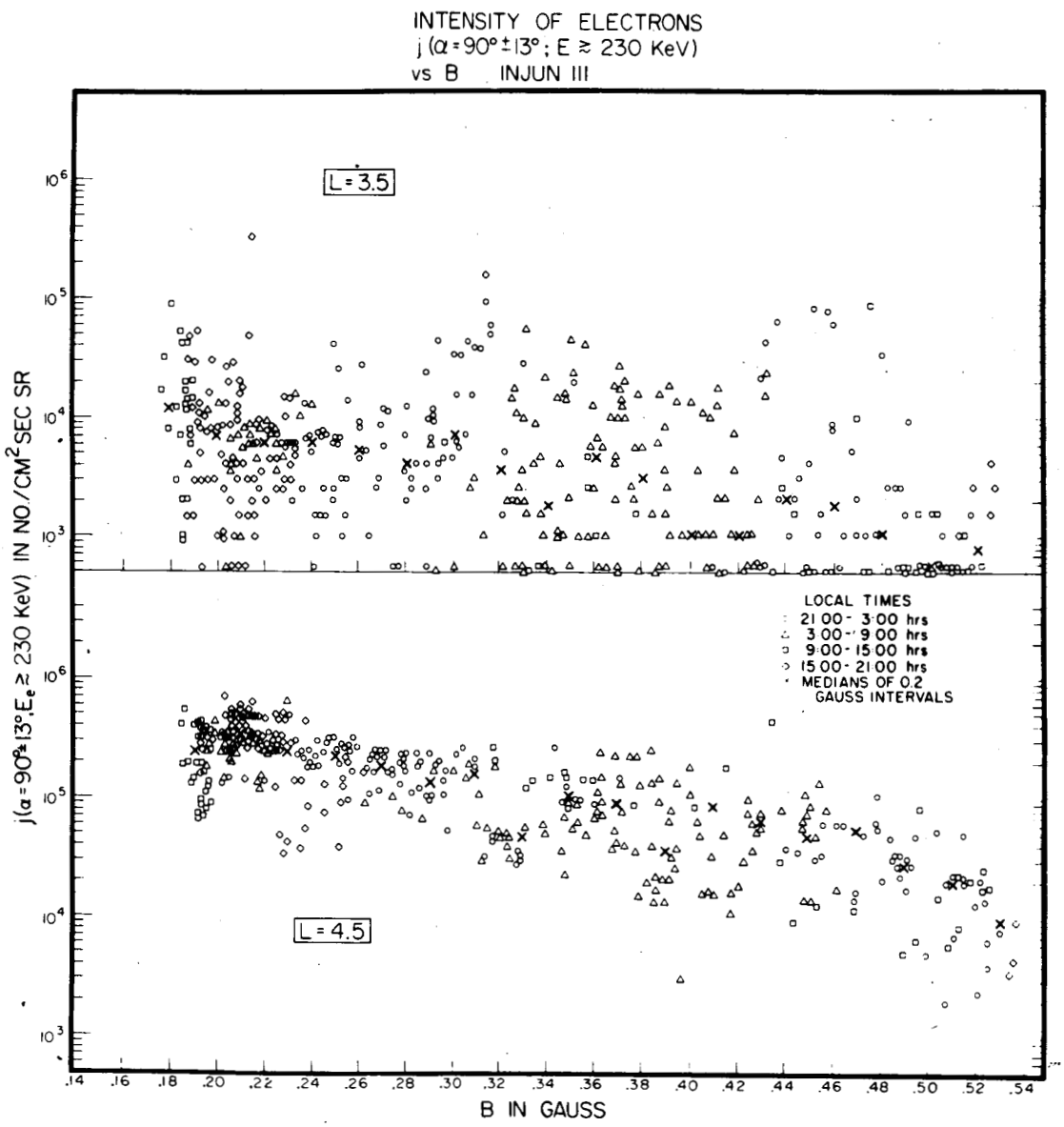
INTENSITY OF ELECTRONS
j (α = 90° ± 13° ; E ≳ 230 KeV)
vs B INJUN III
L = 3.5
L = 4.5
LOCAL TIMES
21 00 - 3 00 hrs
3 00 - 9 00 hrs
9 00 - 15 00 hrs
15 00 - 21 00 hrs
MEDIANS OF 0.2 GAUSS INTERVALS
j(α = 90° ± 13°, E_e ≳ 230 KeV) IN NO/CM² SEC SR
B IN GAUSS

FIGURE 22

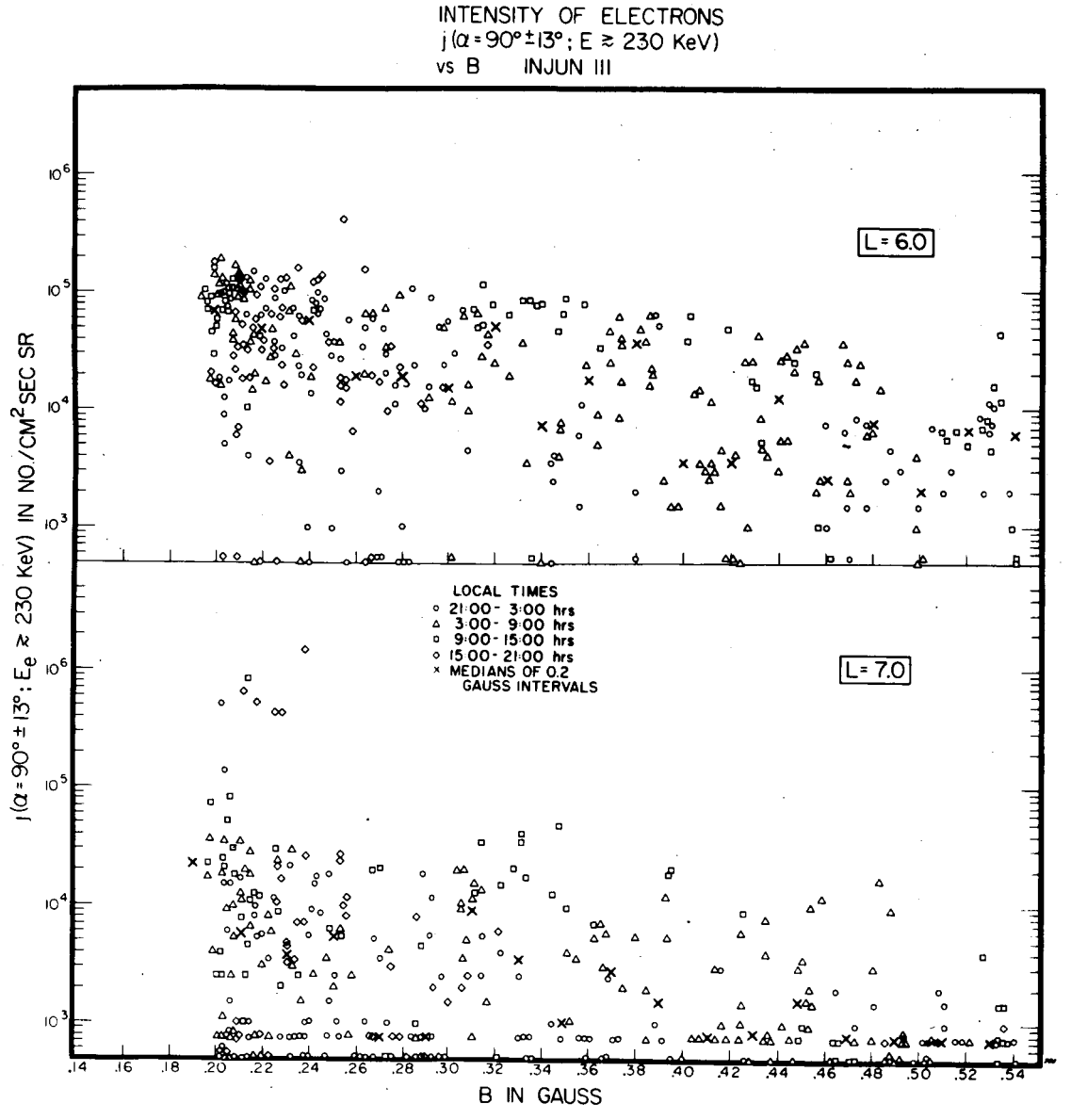
INTENSITY OF ELECTRONS
j(α = 90° ± 13°; E ≳ 230 KeV)
vs B INJUN III
L = 6.0
L = 7.0
LOCAL TIMES
21:00 - 3:00 hrs
3:00 - 9:00 hrs
9:00 - 15:00 hrs
15:00 - 21:00 hrs
MEDIANS OF 0.2 GAUSS INTERVALS
j(α = 90° ± 13°; Ee ≳ 230 KeV) IN NO./CM2SEC SR
B IN GAUSS

FIGURE 23

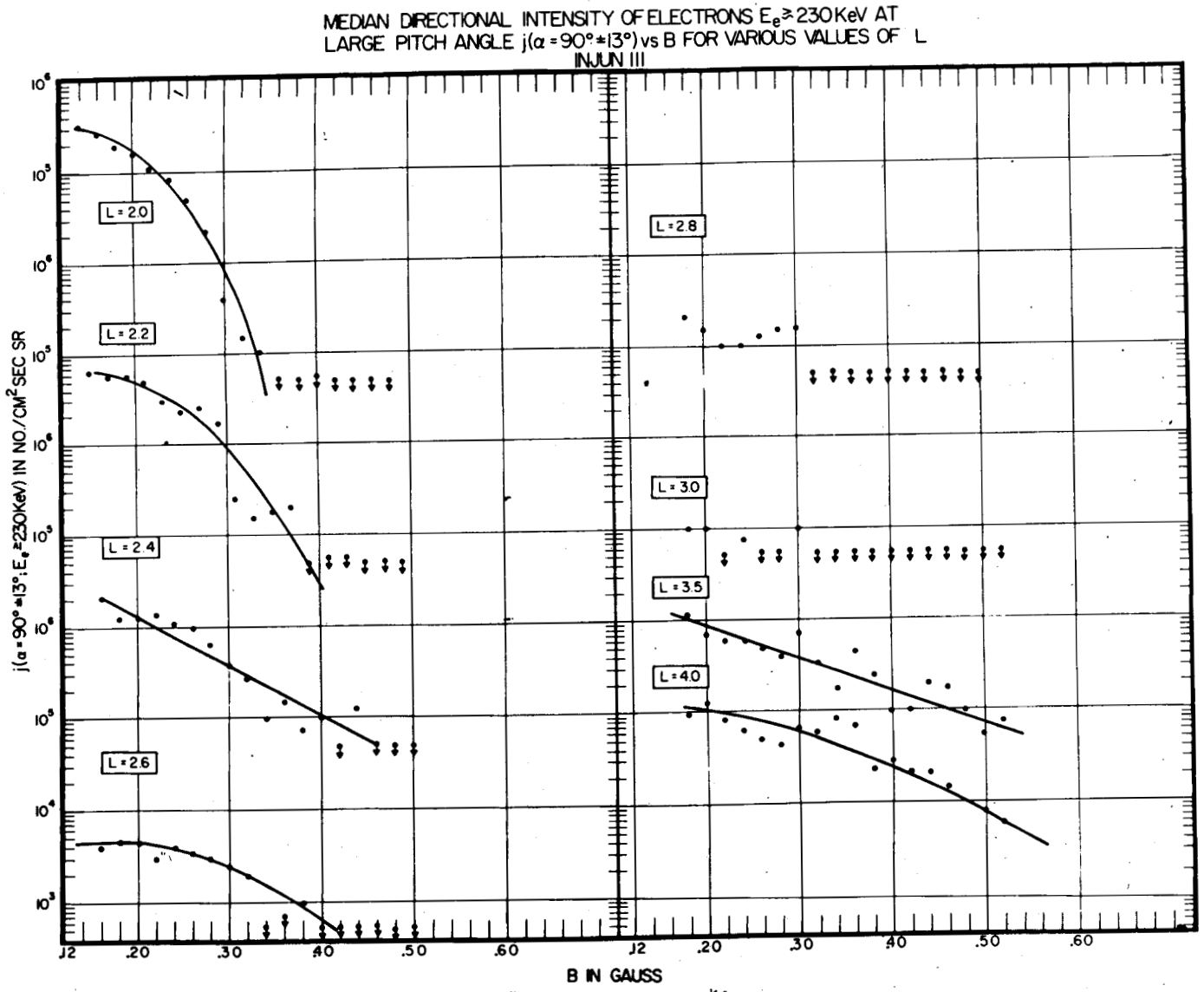
MEDIAN DIRECTIONAL INTENSITY OF ELECTRONS $E_e \geq 230$ KeV AT LARGE PITCH ANGLE $j(\alpha = 90° \pm 13°)$ vs B FOR VARIOUS VALUES OF L
INJUN III
L = 2.0
L = 2.2
L = 2.4
L = 2.6
L = 2.8
L = 3.0
L = 3.5
L = 4.0
$j(\alpha = 90° \pm 13°; E_e \geq 230 KeV)$ IN NO./CM^2 SEC SR
B IN GAUSS
.12
.20
.30
.40
.50
.60

FIGURE 24

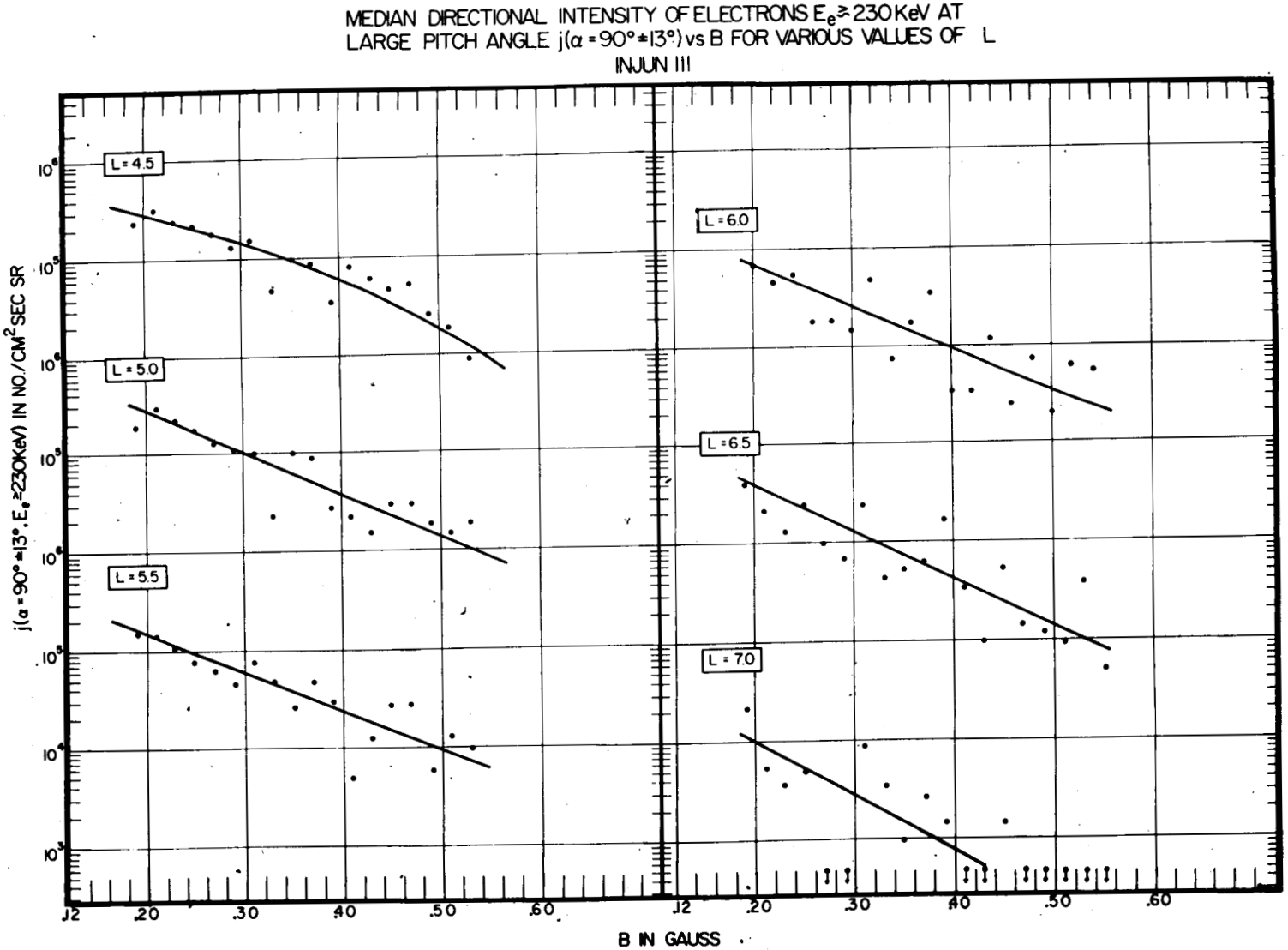
MEDIAN DIRECTIONAL INTENSITY OF ELECTRONS $E_e \geq 230$ KeV AT LARGE PITCH ANGLE $j(\alpha = 90° \pm 13°)$ vs B FOR VARIOUS VALUES OF L
INJUN III
L = 4.5
L = 5.0
L = 5.5
L = 6.0
L = 6.5
L = 7.0
$j(\alpha = 90° \pm 13°, E_e \geq 230 KeV)$ IN NO./CM^2 SEC SR
B IN GAUSS

FIGURE 25

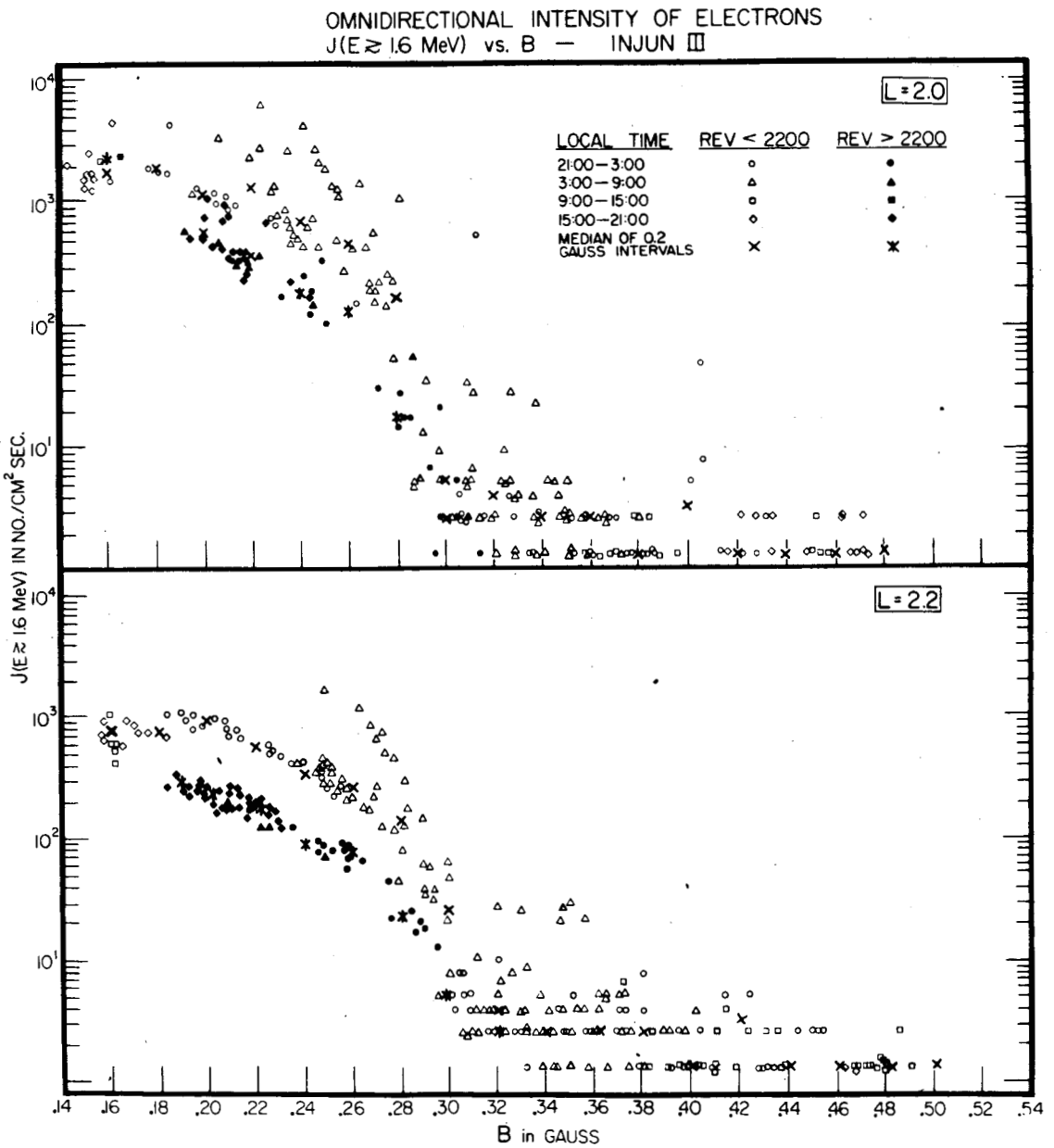
OMNIDIRECTIONAL INTENSITY OF ELECTRONS
J(E≳ 1.6 MeV) vs. B — INJUN III
L = 2.0
LOCAL TIME
REV < 2200
REV > 2200
21:00–3:00
3:00–9:00
9:00–15:00
15:00–21:00
MEDIAN OF 0.2 GAUSS INTERVALS
L = 2.2
J(E≳ 1.6 MeV) IN NO./CM² SEC.
B in GAUSS
.14 .16 .18 .20 .22 .24 .26 .28 .30 .32 .34 .36 .38 .40 .42 .44 .46 .48 .50 .52 .54

FIGURE 26

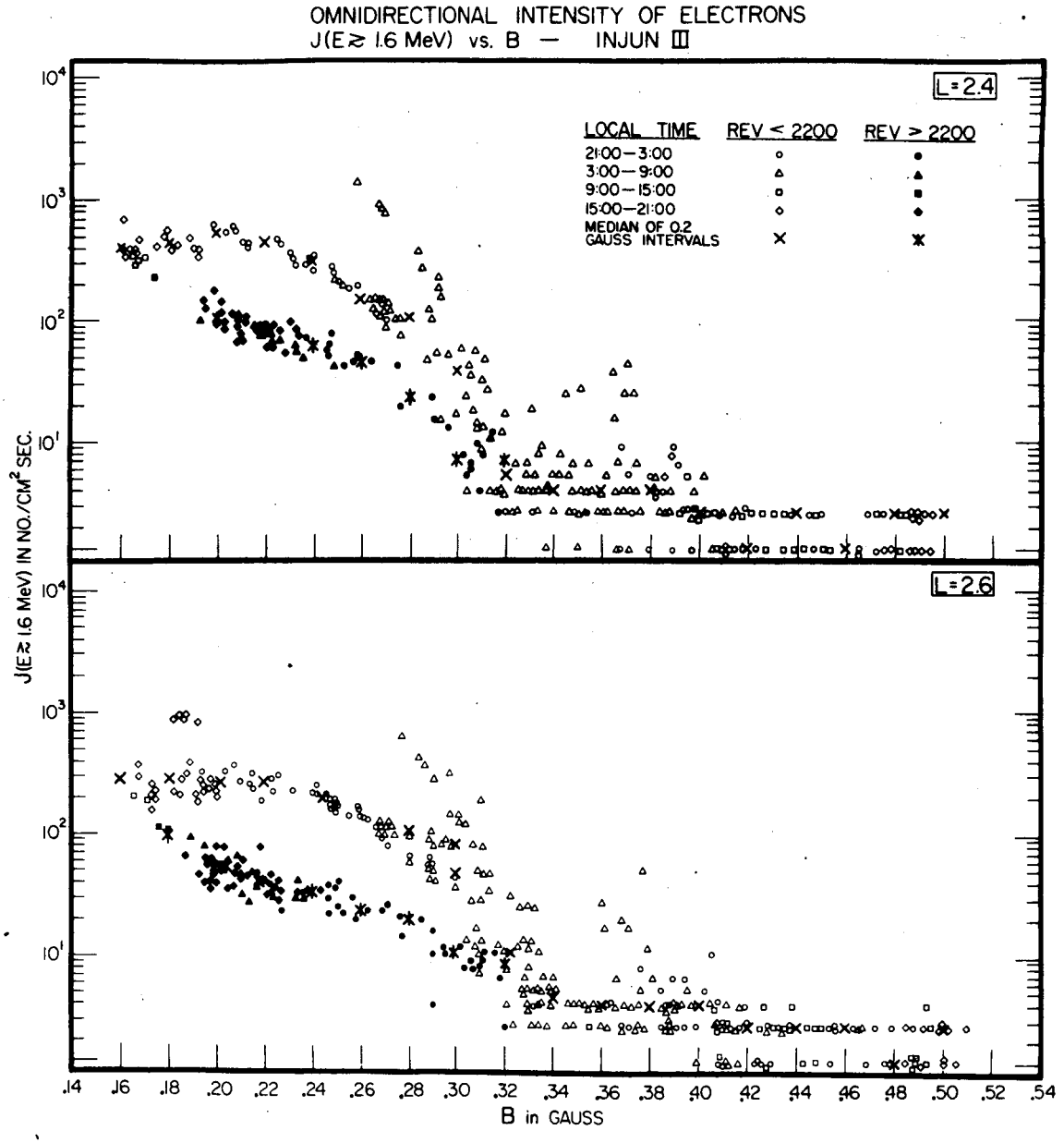
OMNIDIRECTIONAL INTENSITY OF ELECTRONS
J(E≳ 1.6 MeV) vs. B — INJUN III
L=2.4
LOCAL TIME
REV < 2200
REV > 2200
21:00—3:00
3:00—9:00
9:00—15:00
15:00—21:00
MEDIAN OF 0.2 GAUSS INTERVALS
L=2.6
J(E≳ 1.6 MeV) IN NO./CM² SEC.
B in GAUSS

FIGURE 27

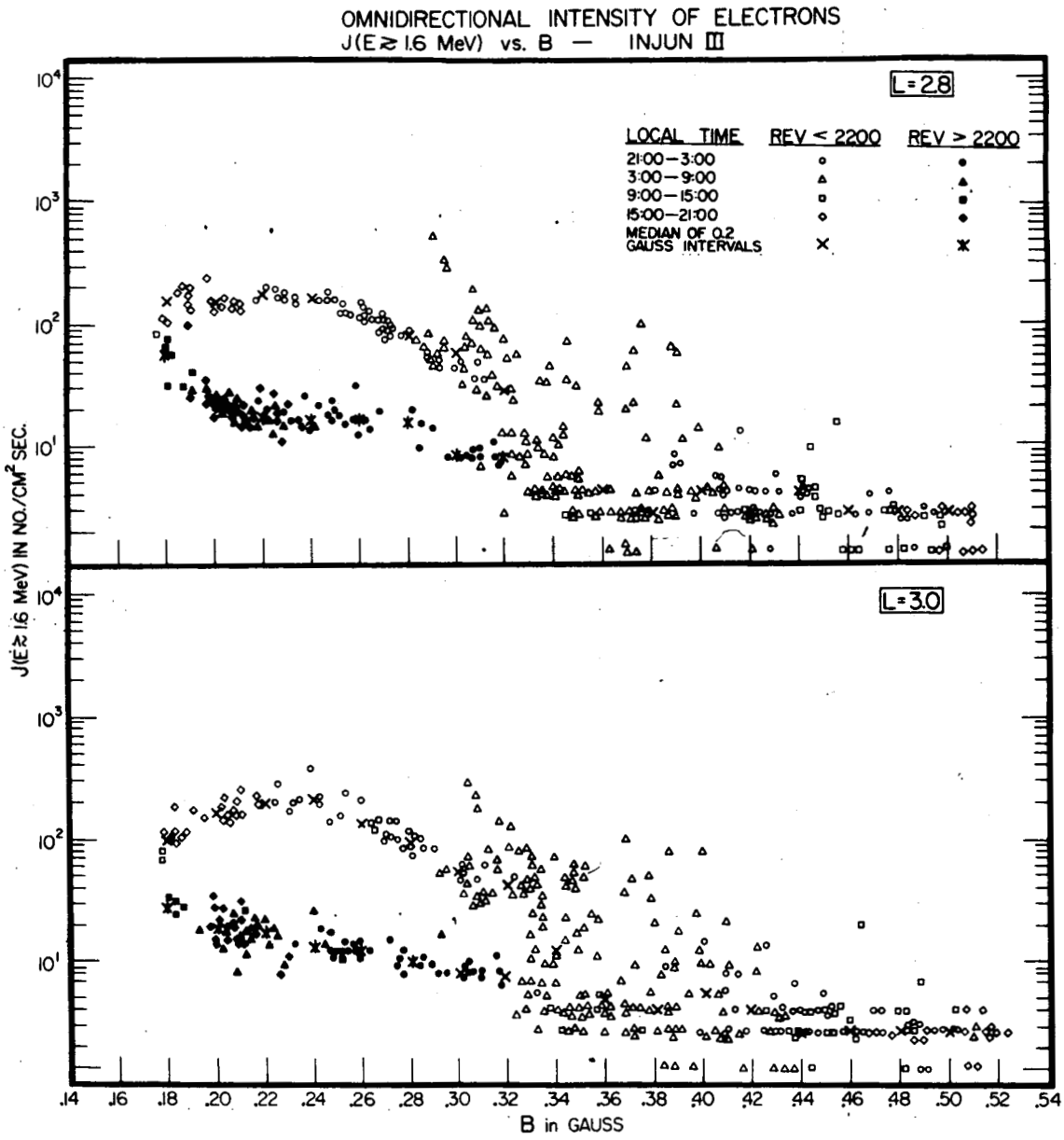
OMNIDIRECTIONAL INTENSITY OF ELECTRONS
J(E ≳ 1.6 MeV) vs. B — INJUN III
L = 2.8
L = 3.0
LOCAL TIME
REV < 2200
REV > 2200
21:00 – 3:00
3:00 – 9:00
9:00 – 15:00
15:00 – 21:00
MEDIAN OF 0.2 GAUSS INTERVALS
J(E ≳ 1.6 MeV) IN NO./CM² SEC.
B in GAUSS

FIGURE 28

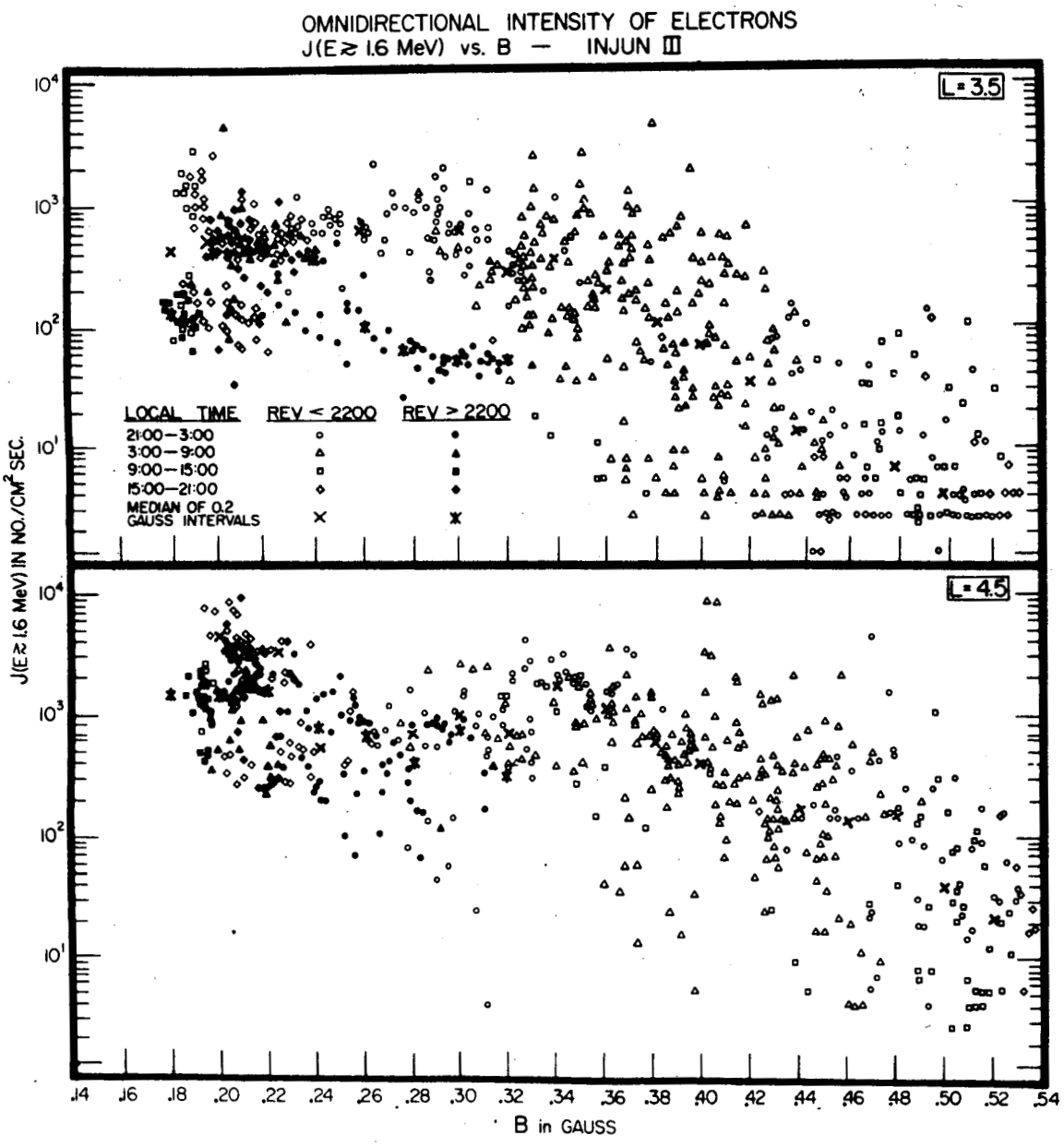
OMNIDIRECTIONAL INTENSITY OF ELECTRONS
J(E≥ 1.6 MeV) vs. B — INJUN III
L=3.5
L=4.5
LOCAL TIME
REV < 2200
REV > 2200
21:00–3:00
3:00–9:00
9:00–15:00
15:00–21:00
MEDIAN OF 0.2 GAUSS INTERVALS
J(E≥ 1.6 MeV) IN NO./CM² SEC.
B in GAUSS

FIGURE 29

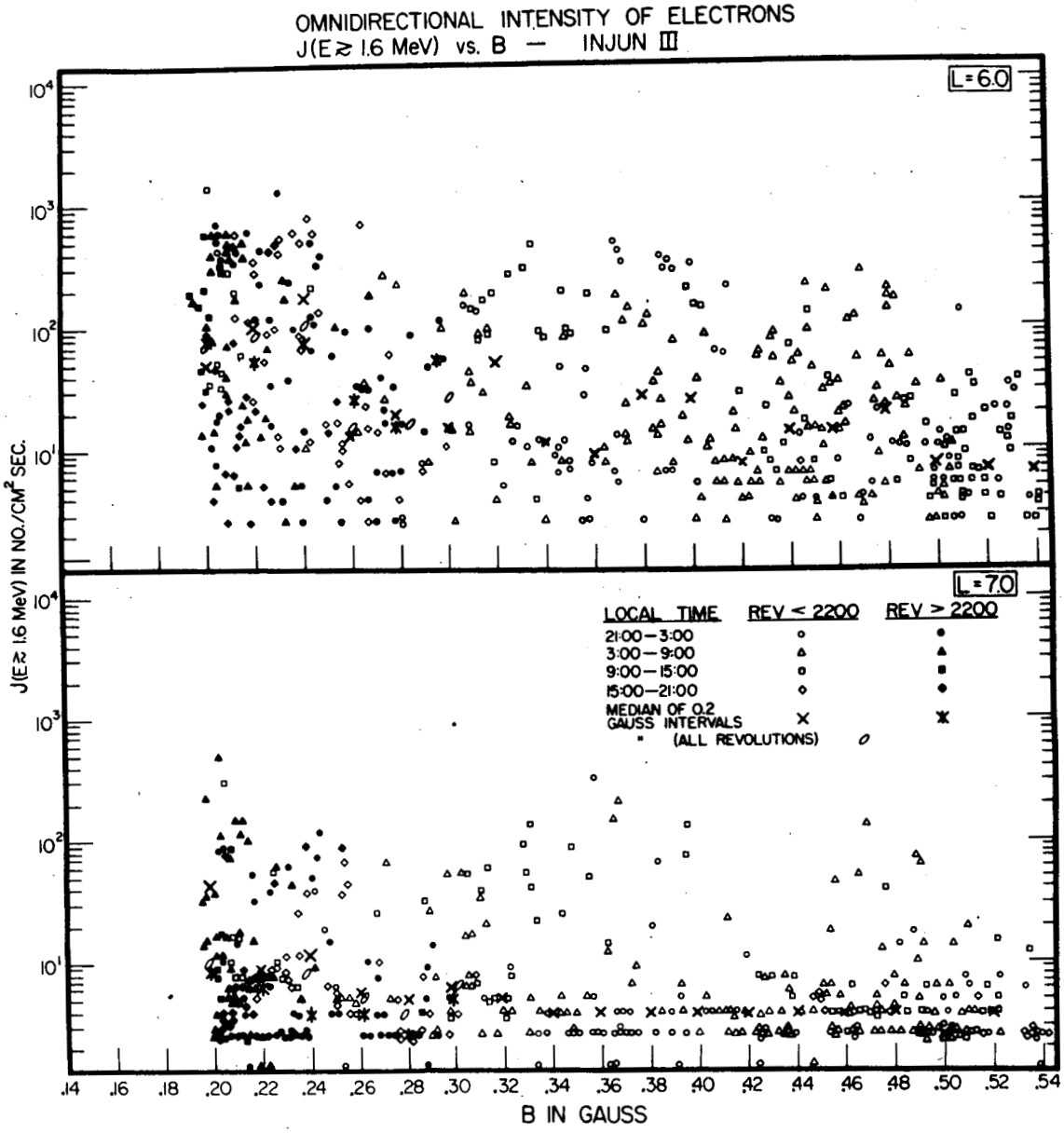
OMNIDIRECTIONAL INTENSITY OF ELECTRONS
J(E≳ 1.6 MeV) vs. B — INJUN III
L=6.0
L=7.0
J(E≳ 1.6 MeV) IN NO./CM² SEC.
LOCAL TIME
REV < 2200
REV > 2200
21:00–3:00
3:00–9:00
9:00–15:00
15:00–21:00
MEDIAN OF 0.2 GAUSS INTERVALS
(ALL REVOLUTIONS)
B IN GAUSS

FIGURE 30

MEDIAN OMNIDIRECTIONAL INTENSITY OF ELECTRONS

$E_e \geq 1.6$ MeV J vs B. FOR VARIOUS VALUES OF L

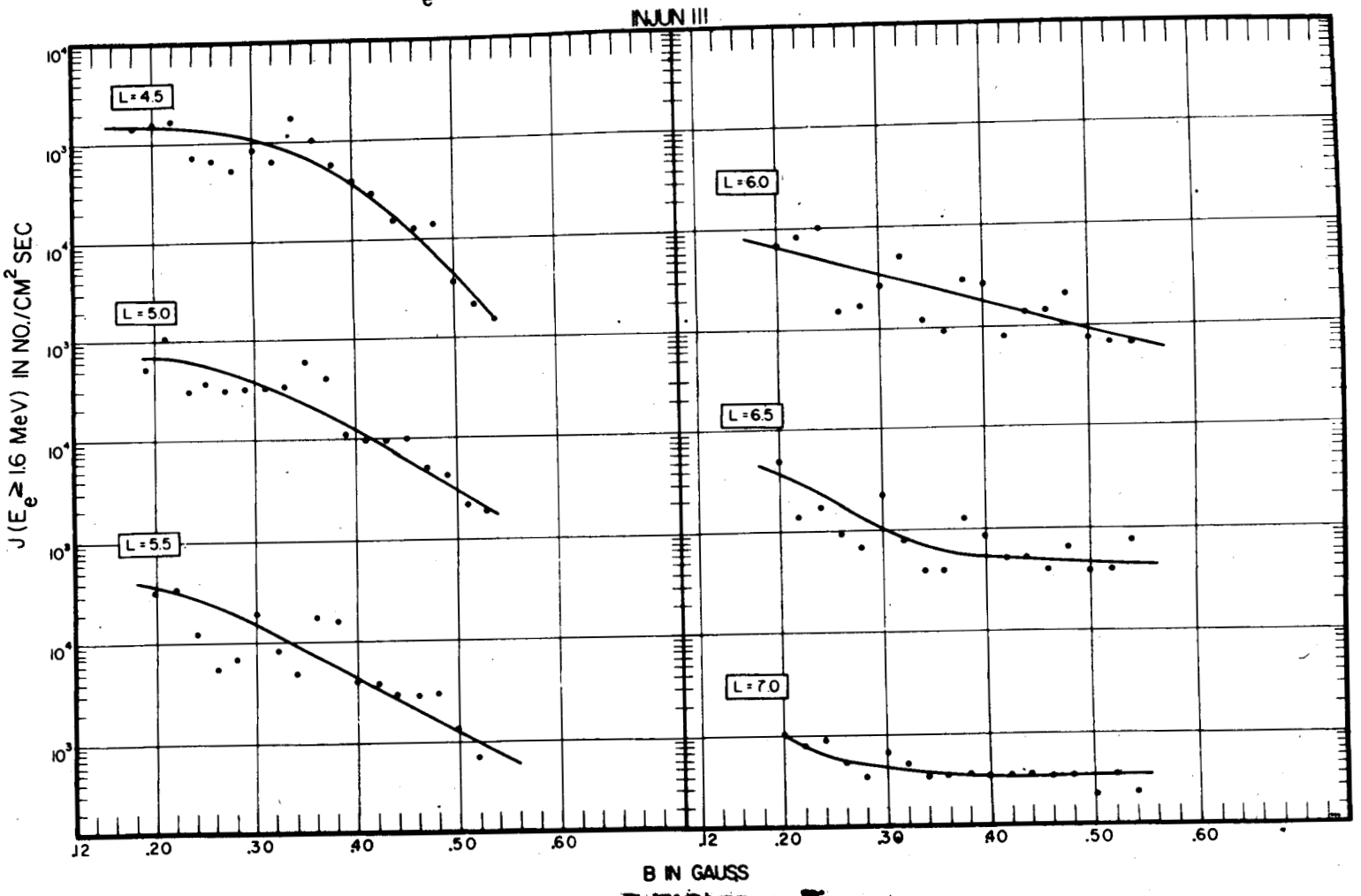

FIGURE 31

LATITUDE PROFILE OF THE OMNIDIRECTIONAL INTENSITY OF 1.6 MeV ELECTRONS
AT B = 0.30 GAUSS DERIVED FROM INTENSITY VS. B CURVES

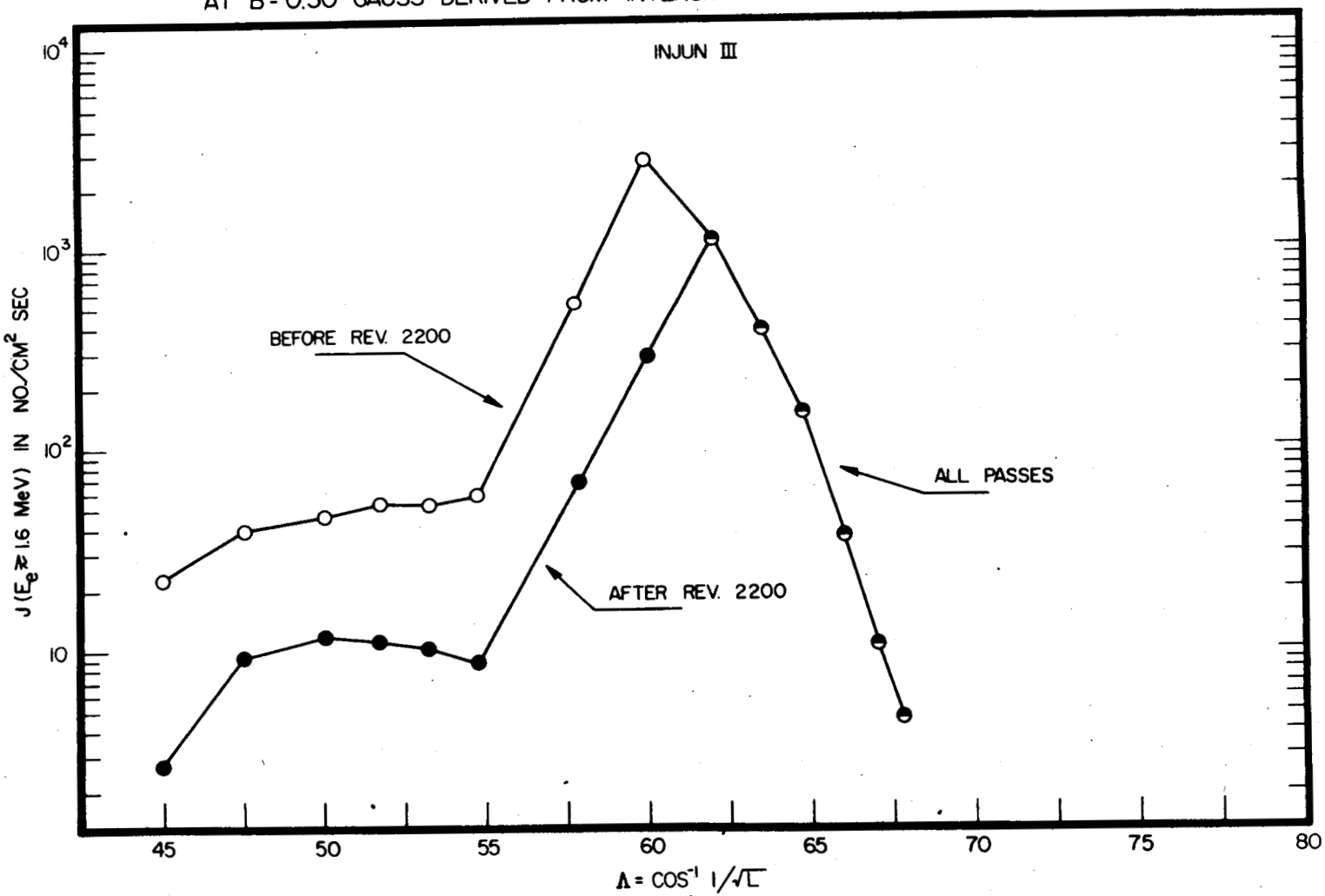

FIGURE 32

PLOTS OF INTENSITY VS L FOR REVOLUTION 2022 INJUN III

MAY 24,1963 K_P = 0+ K_P 24 HR. SUM = 3-

L		2.0	2.5	3.0	3.5	4.0	4.5	5.0	5.5	6.0	6.5	7.0	7.5
UNIVERSAL TIME	NORTHBOUND	19:05:29	19:07:27	19:08:54	19:10:01	19:10:71	19:11:40	19:12:20	19:12:53	19:13:25	19:13:52	19:14:18	19:14:60
	SOUTHBOUND	19:46:28	19:42.13	19:39:30	19:37:32	19:36:01	19:34:39	19:33:48	19:33:20	19:32:12	19:31:34	19:30.27	19:29:00
LOCAL TIME	NORTHBOUND	5:37	6:00	6:19	6:37	6:52	7:08	7:22	7:35	7:48	8:00	8:12	9:59
	SOUTHBOUND	15:36	15:20	15:08	14:59	14:51	14:44	14:38	14:32	14:26	14:21	14:17	14:12
B	NORTHBOUND	.304	.302	.300	.300	.297	.293	.291	.289	.287	.285	.284	.283
	SOUTHBOUND	.144	.162	.174	.182	189	.195	.199	.203	.206	.209	.212	.214

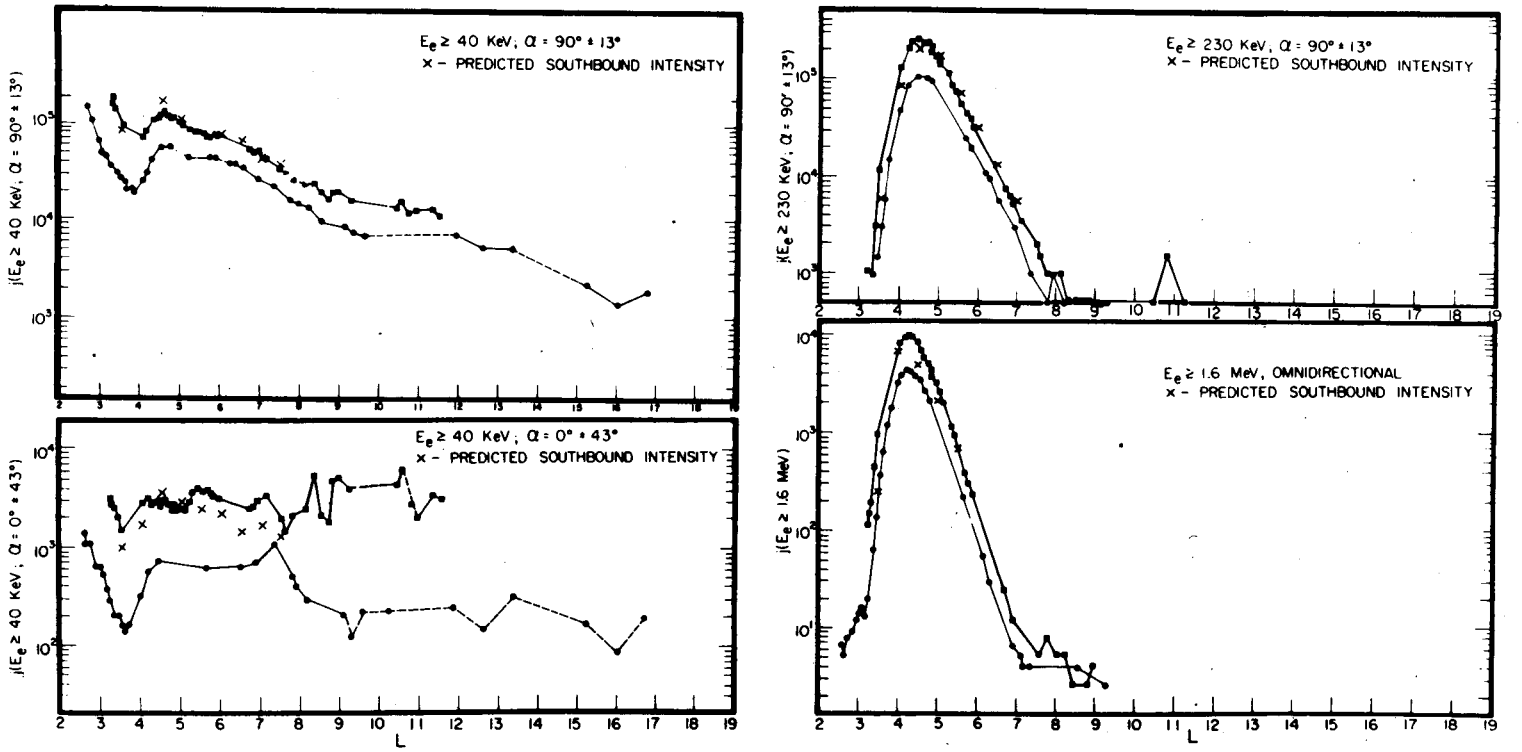

FIGURE 33

PLOTS OF INTENSITY VS L FOR REVOLUTION 1886 INJUN III

MAY 13, 1964 $K_p = 3^+$ K_p 24 HR. SUM = 28°

L		2.0	2.5	3.0	3.5	4.0	4.5	5.0	5.5	6.0	6.5	7.0	7.5
UNIVERSAL TIME	NORTHBOUND	21:51:30	21:53:24	21:54:47	21:55:53	21:56:47	21:57:33	21:58:13	21:58:67	21:59:20	21:79:68	22:00:16	22:00:61
	SOUTHBOUND	22:30:21	22:26:00	22:23:15	22:21:17	22:19:46	22:18:33	22:17:32	22:16:39	22:15:76	22:15:17	22:14:58	22:14:03
LOCAL TIME	NORTHBOUND	7:39	8:03	8:24	8:44	9:03	9:20	9:37	9:52	10:08	10:23	10:37	10:51
	SOUTHBOUND	17:33	17:17	17:05	16:55	16:47	16:39	16:32	16:26	16:21	16:15	16:10	16:04
B	NORTHBOUND	.343	.338	.333	.328	.324	.320	.317	.314	.311	.308	.306	.303
	SOUTHBOUND	.146	.168	.182	.193	.201	.208	.214	.218	.222	.227	.230	.233

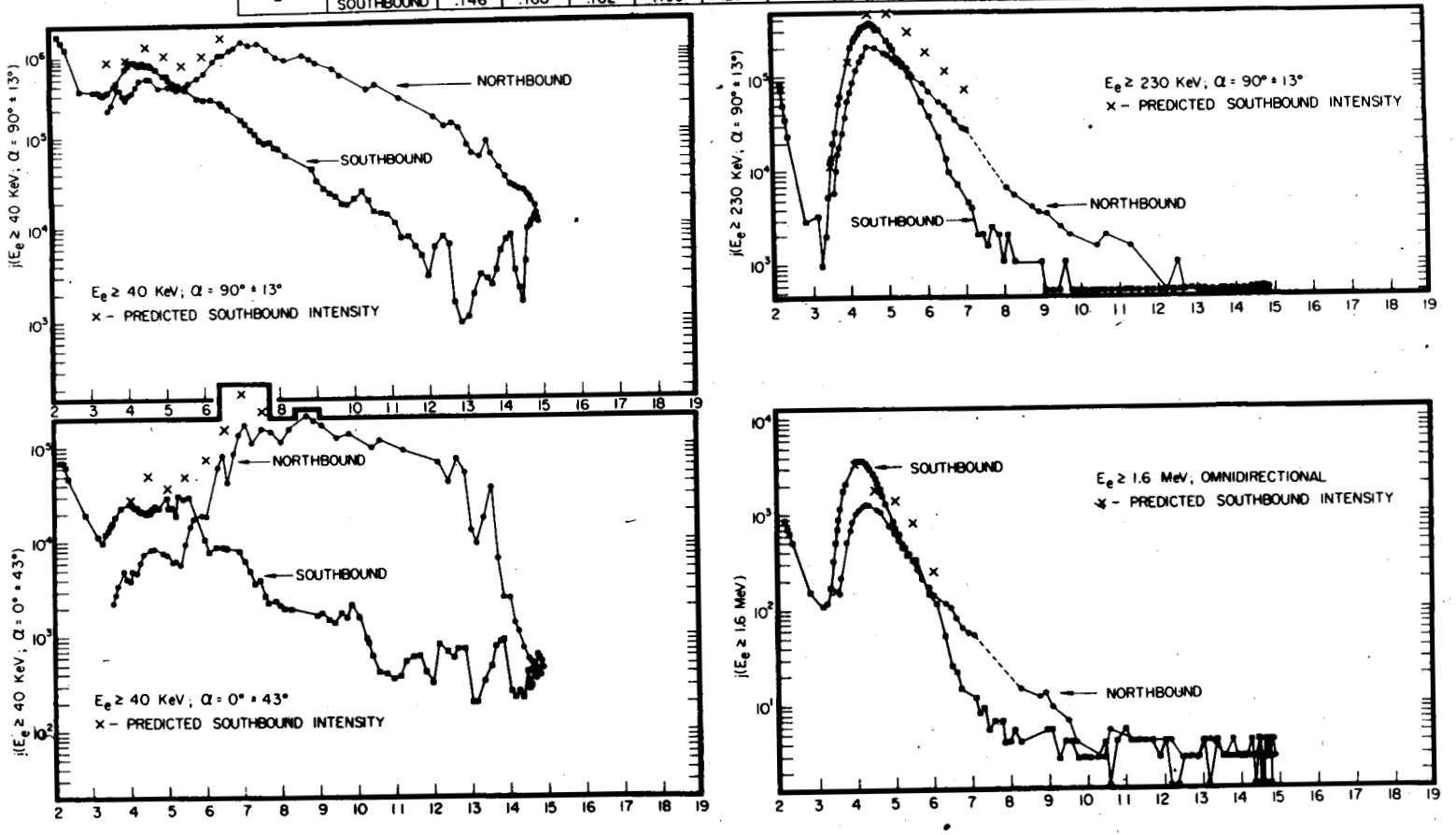

FIGURE 34